GPS zenith delay sensitivity evaluated from high-resolution numerical weather prediction simulations of the 8–9 September 2002 flash flood over southeastern France

Hugues Brenot, Véronique Ducrocq, Andrea Walpersdorf, Cedric Champollion, Olivier Caumont

JOURNAL OF GEOPHYSICAL RESEARCH, VOL. 111, D15105, doi:10.1029/2004JD005726, 2006

GPS zenith delay sensitivity evaluated from high-resolution numerical weather prediction simulations of the 8–9 September 2002 flash flood over southeastern France

Hugues Brenot,[1,2] Véronique Ducrocq,[1] Andrea Walpersdorf,[2] Cédric Champollion,[3] and Olivier Caumont[1]

Received 21 December 2004; revised 21 December 2005; accepted 13 March 2006; published 10 August 2006.

[1] Estimations of zenith total delays (ZTD) were obtained during postprocessing of a high-resolution (2.4 km) nonhydrostatic atmospheric model (Méso-NH). These estimations were used to determine their sensitivity with respect to formulations of atmospheric refractivity, the approximation of zenith hydrostatic delays (ZHD) deduced from ground pressure, and the contributions of hydrometeors. The factor κ for the conversion of zenith wet delay (ZWD) to integrated water vapor (IWV) was examined. Méso-NH is applied here to the extreme flash flood event of 8–9 September 2002 in southeastern France. The use of the hydrostatic formulation (to infer ZHD) leads to an overestimation of up to 18 mm with respect to the vertical integration of refractivity. Delay contributions of hydrometeors simulated by the high-resolution model reached more than 70 mm ($\approx$11 kg/m^2 IWV) in the heart of the convective cells in the case of the extreme flood event. The mean variations of IWV due to the use of different conversion factors (κ used to transform ZWD to IWV) are evaluated to be less than 0.3 kg/m^2. This is less than the mean underestimation of IWV by 0.6 kg/m^2 relative to the GPS-like evaluation of IWV using the hydrostatic formulation and the ground temperature. In this study we also use GPS ZTD observations to validate three different numerical simulations of this extreme flood event. The simulation with the best fit to the GPS observations is also in best agreement with the surface rainfall measurements.

Citation: Brenot, H., V. Ducrocq, A. Walpersdorf, C. Champollion, and O. Caumont (2006), GPS zenith delay sensitivity evaluated from high-resolution numerical weather prediction simulations of the 8–9 September 2002 flash flood over southeastern France, *J. Geophys. Res.*, *111*, D15105, doi:10.1029/2004JD005726.

1. Introduction

[2] The method to estimate the integrated water vapor content (IWV), extracted from initial GPS observations of zenith total delay (ZTD) and ground pressure, has been presented by *Bevis et al.* [1992] and *Businger et al.* [1996]. By comparing measurements from GPS stations with those from other observational systems (microwave water vapor radiometry, radiosounding, very long baseline interferometry) [*Bevis et al.*, 1992; *Rocken et al.*, 1993, 1994; *Tregoning et al.*, 1998; *Niell et al.*, 2001], GPS data have proved to be as valuable in estimating IWV (with an accuracy of 1–2 kg/m^2). GPS water vapor observations are available several times per hour [*Gendt et al.*, 2004]. They permit (1) the validation of numerical weather prediction (NWP) systems [*Yang et al.*, 1999; *Cucurull et al.*, 2000; *Köpken*, 2001; *Vey et al.*, 2004; *Bock et al.*, 2005], (2) providing a climatology of tropospheric water vapor [*Stoew and Elgered*, 2004], and (3) improving the knowledge of mesoscale phenomena [*Liou and Huang*, 2000; *Cucurull et al.*, 2002].

[3] This paper contributes to the studies of the "Observatoire Hydrométéorologique Méditerranéen-Cévennes-Vivarais" (OHM-CV) [*Delrieu et al.*, 2005], which aims to understand and improve the forecast of frequent flash flood events over the Cévennes-Vivarais region close to the Mediterranean coast in southeastern France (100 km to the northwest of Marseille, Figure 1). In this framework, the 8–9 September 2002 extreme flash flood event has been simulated with a high-resolution nonhydrostatic model (Méso-NH) [*Ducrocq et al.*, 2004]. This extreme flash flood event took place over southeastern France (Gard region) and was characterized by an extreme precipitating convective event, exhibiting both high hydrometeor contents and nonhydrostatic effects due to convective upward and downward

[1] Centre Nationale de Recherches Meteorologique, Groupe de Meteorologie Moyenne Echelle, Modélisation et Initialisation de la Convection en synergie avec l'Analyse des Données Observées, Météo-France, Toulouse, France.
[2] Laboratoire de Géophysique Interne et de Tectonophysique, Maison des Géosciences, CNRS, Université Joseph Fourier, Grenoble, France.
[3] Laboratoire Dynamique de la Lithosphère, CNRS, Université de Montpellier II, Montpellier, France.

0148-0227/06/2004JD005726$09.00

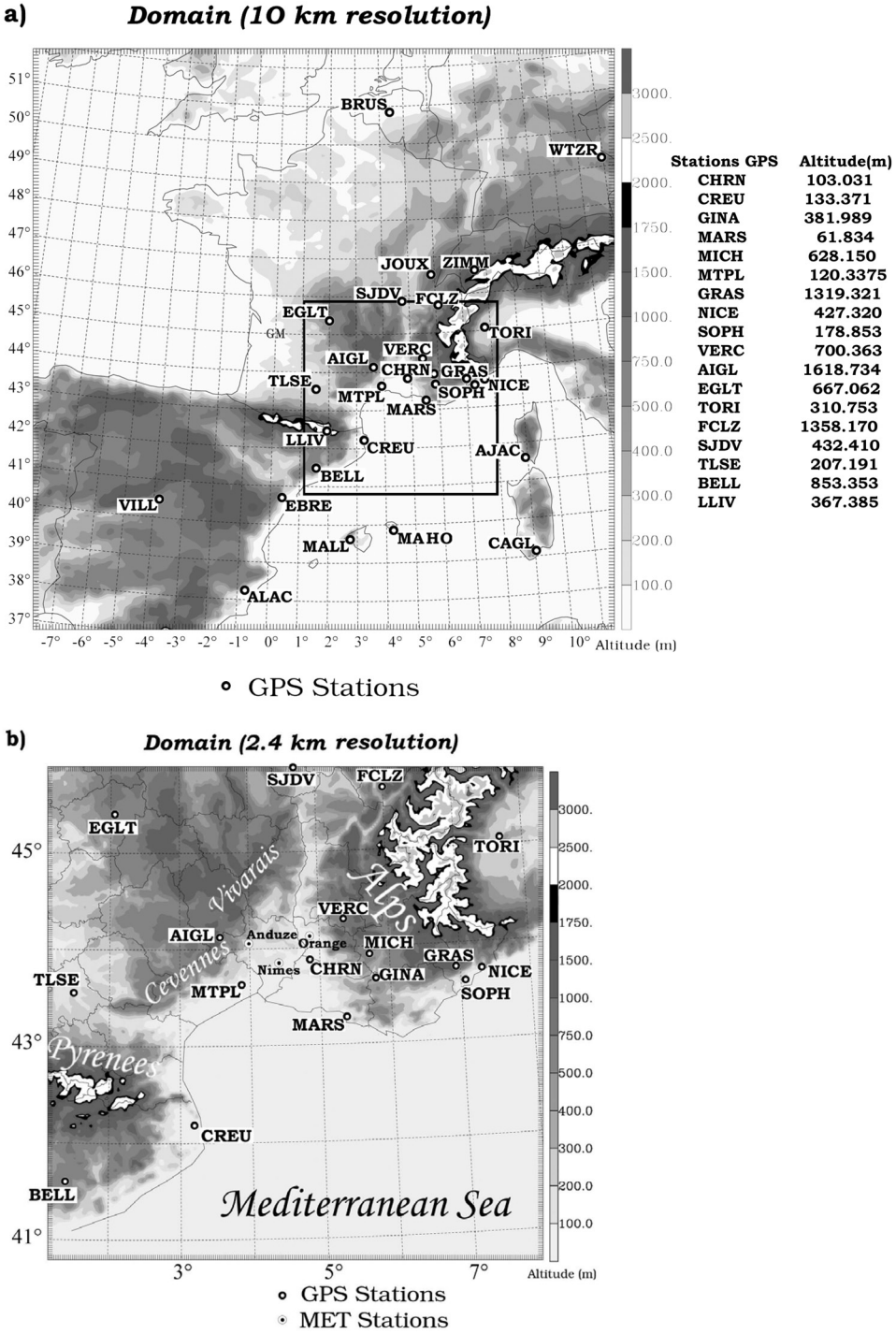

Figure 1. Locations of the GPS sites (text in white boxes) shown for the two Méso-NH domains: (a) the 9.5-km resolution domain and its orography (black box situates the 2.4-km domain) and (b) the 2.4-km resolution domain. The altitudes of the GPS stations are indicated on the right of Figure 1a. Some additional geographical locations are indicated on Figure 1b (sea, mountain ranges, and three meteorological stations referred to in the text). The thin lines delineate the French departments. MARS corresponds to the GPS station of Marseille.

motions. Méso-NH simulations of this event have been postprocessed to quantify of the sensitivity to the formulation of the tropospheric refractivity, from which the GPS ZTD and IWV are derived. We have especially examined the impact of nonhydrostatic effects and of hydrometeors on ZTD estimation.

[4] The evaluation and the understanding of atmospheric refractivity has been studied by several authors [e.g.,

Boudouris, 1963; *Bean and Dutton*, 1966; *Owens*, 1967; *Saastamoinen*, 1973a, 1973b, 1973c]. Generally, they describe microwave propagation with three atmospheric refractivity coefficients ($N = N(k_1, k_2, k_3)$), in an atmospheric medium evolving with a temperature, T, an absolute pressure, P, and a water vapor partial pressure, e. Several sets of (k_1, k_2, k_3) values have been proposed in the past [*Smith and Weintraub*, 1953; *Essen and Froome*, 1963; *Thayer*, 1974; *Hasegawa and Stokesberry*, 1975; *Bevis et al.*, 1994]. Therefore, as a first step in our study, uncertainties of ZTD estimations referring to different physical expressions of refractivity have been evaluated. An expression for the atmospheric coefficients that depends on pressure and temperature, following *Saastamoinen* [1973b], has also been tested. Then, as proposed by [*Kursinski et al.*, 1997; *Solheim et al.*, 1999; *Hajj et al.*, 2002], a contribution induced by the hydrometeors has been added in the refractivity formulation and its impact on the ZTD estimation evaluated. In a second step, sensitivity of the relationships between ZTD, ZWD, and IWV have been studied referring to *Bevis et al.* [1992] and *Emardson and Derks* [1999]. The conversion formulae are dependent on site or region. With the high-resolution nonhydrostatic simulations we can examine the validity of the formulae used to derive IWV from ZTD and their associated assumptions (hydrostatic state, surface temperature dependency). Then, knowing the sensitivity to the refractivity formulations and to the IWV-ZWD-ZTD formula, section 3 illustrates how GPS measurements from a mesoscale network may be helpful in validating high-resolution simulations, with differing initial conditions.

[5] In the following, we introduce the GPS data and analysis, the flash flood event, the Méso-NH simulations and the assessments of ZTD, ZWD and IWV from model outputs. Then, the results of the sensitivity tests are shown as one outcome of our study. The second outcome is the comparison of simulated ZTD with GPS measurements for the validation of the simulations of 8–9 September 2002 event.

2. Data and Numerical Simulations

2.1. GPS Network and Data Analysis

[6] Data from 35 GPS stations have been processed (Figure 1): stations AIGL, CHRN, FCLZ, GINA, JOUX, MICH, MTPL, NICE, SJDV and SOPH from the REGAL (Réseau GPS permanent dans les Alpes) network (http://kreiz.unice.fr/regal/), stations AJAC, EGLT, GRAS, MARS and TLSE from the national French permanent network RGP (http://lareg.ensg.ign.fr/RGP/index.html), stations SJDS and VERC from the semipermanent network VENICE in south of France [*Masson et al.*, 2003], stations BELL, CREU, EBRE, LLIV from the regional Spanish network CATNET (http://draco.icc.es/geofons/catnet/en/home.php), and station MAHO in the Baleares maintained by the Royal Observatory of Spain; stations ALAC, BOR1, BRUS, CAGL, GRAZ, MALL, MATE, ONSA, POTS, TORI, VILL, WTZR and ZIMM from the EUREF network (http://www.epncb.oma.be/index.html) are included in the data analysis as fiducial stations for the realization of the reference frame. The GPS data analysis has been performed using the GAMIT software (version 10.07, *King and Bock* [2000]). The primary analysis provides precise coordinates for the local stations for each 24 h of measurements. In this step, tropospheric parameters have been estimated with a 2 hourly resolution. The repeatabilities of the unconstrained daily GAMIT solution for all baseline components are 1.2 mm, 2.1 mm and 4.7 mm for the north, east and vertical components, respectively. The final positions of the stations in the ITRF2000 reference frame [*Altamimi et al.*, 2002] are obtained in a global solution using the Kalman filter, GLOBK [*Herring et al.*, 1990]. The reference frame is established by constraining the positions of 13 fiducial GPS stations to their ITRF2000 values. In a secondary analysis, zenith delays are calculated every 30 minutes and horizontal tropospheric gradients (NS and EW components) are estimated hourly. Baselines greater than 2000 km have been used in order to decorrelate the tropospheric parameters from vertical position estimations [*Tregoning et al.*, 1998]. Loose constraints have been applied on the station coordinates obtained in the primary analysis (1 m on horizontal and 2 m on vertical). The tropospheric parameters of the ambiguity free solution have been used. ZTD measurements have been produced using a sliding window strategy with sessions of 24 hours of data shifted by 12 hours. Only the middle 12 hours of each session have been retained (for more details, see *Champollion et al.* [2004]).

2.2. The 8–9 September 2002 Flash Flood Event

[7] On 8–9 September 2002, a heavy precipitating system affected the Gard region (the region including Nîmes, Anduze, and Orange; see Figure 1): 24 people were killed during this event and the economic damage is estimated at 1.2 billion euros [*Huet et al.*, 2003]. *Delrieu et al* [2005] proposed a detailed description of the meteorological and hydrological event. This paper describes a brief overview. The meteorological environment was characterized by an upper cold low pressure, centered over Ireland, that extended medicinally to the Iberian Peninsula and generated a southwesterly diffluent flow over southeastern France on 8 September 2002 (Figure 2), that progressively evolved in a southerly flow during the night of 8–9 September. Associated with this upper level flow a surface front undulated over western France. Convection formed well ahead of the surface cold front, in the warm sector, where a moist low-level southeasterly flow prevailed (see the window in Figure 2a for the location of the heavy precipitation). Prior to the development of the convection, the atmosphere was conditionally unstable in this region as shown by the midnight Nîmes radiosounding of the 8 September (CAPE of the most unstable parcel about 850 J/kg). IWV computed from this radiosounding shows that the water vapor content of the atmosphere was already high (33 kg/m^2). This value is in the upper ten percent of the distribution of IWV for the Nîmes sounding for September months between 1994 and 2003, the average value being of 22 kg/m^2. After the onset of convection, the 1200 UTC sounding is almost saturated with a water precipitation value of 39 kg/m^2 reaching the upper five percents of the distribution of IWV for the 1994–2003 Nîmes soundings.

[8] Triggered over the Mediterranean Sea during the early morning, the convective cells progressed northward to form inland a quasi-stationary mesoscale convective system

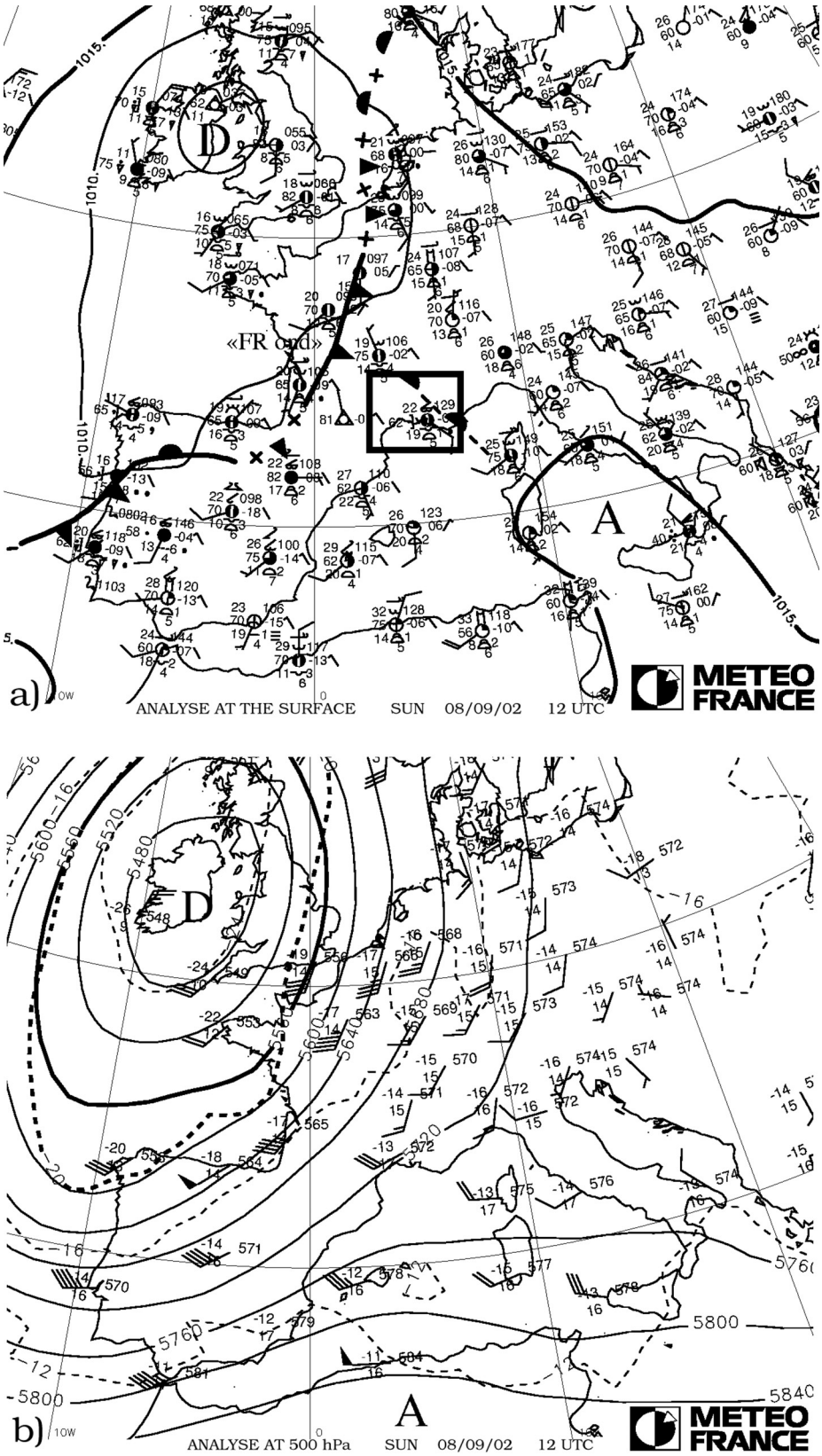

Figure 2. Surface and 500 hPa height analyses from Meteo-France at 1200 UTC on 8 September 2002. (a) Surface analysis: The sea level pressure is shown with D for depression center and A for anticyclone center. The box delineates the area affected by the heavy rainfall event. (b) The 500 hPa analysis: The geopotentials (in m) and temperature (in degrees Celsius) are shown as solid and dashed lines, respectively (A for high center and D for low center of geopotential).

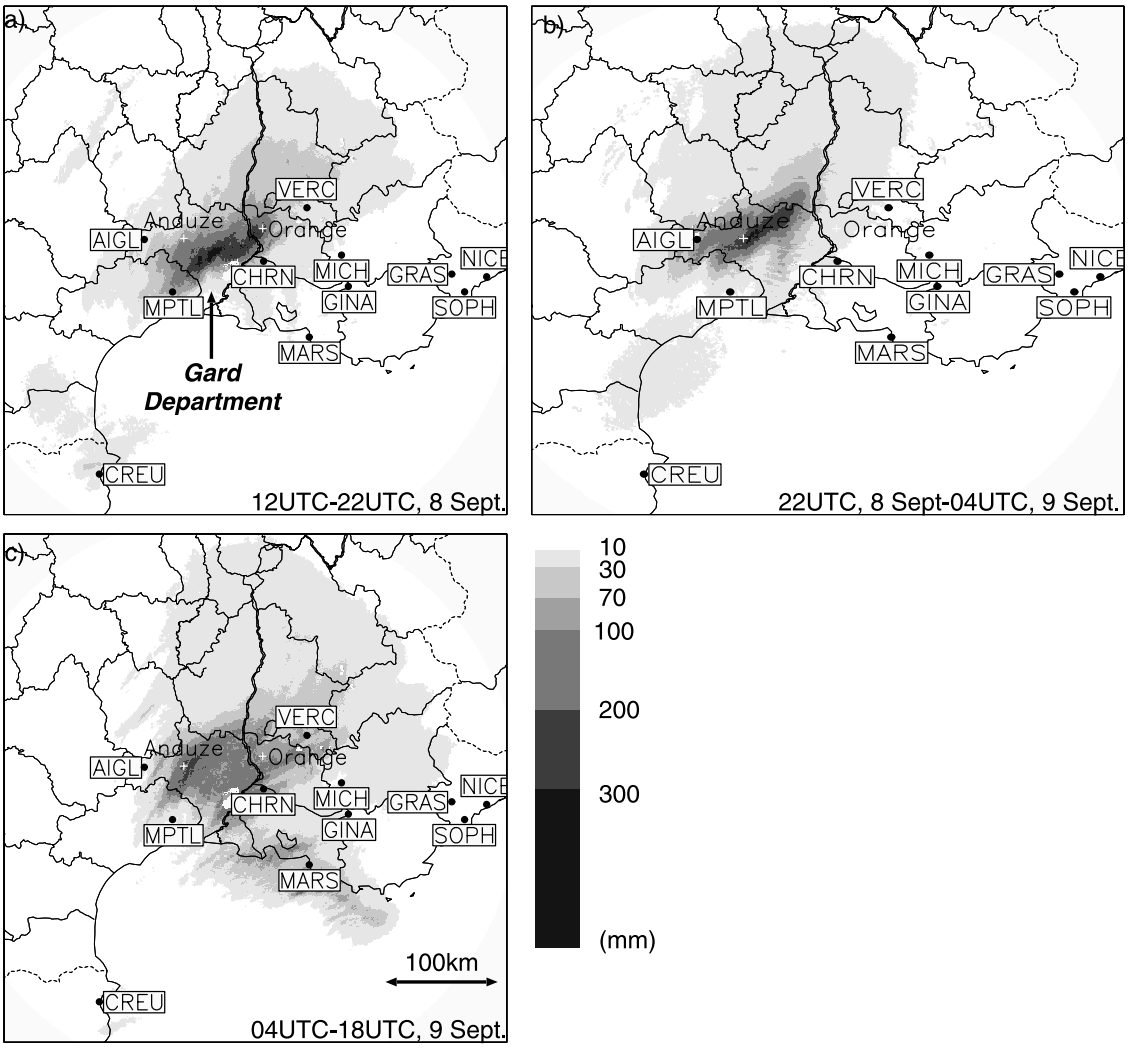

Figure 3. Accumulated rainfall (in mm) from the Nîmes radar: (a) from 1200 to 2200 UTC on 8 September 2002, (b) from 2200 UTC on 8 September 2002 to 0400 UTC on 9 September 2002, and (c) from 0400 to 1800 UTC on 9 September 2002. The thin lines delineate the French departments. Locations of some GPS stations (dots, station names in boxes) and of two rain gauge stations (white crosses) are indicated.

(MCS) over the Gard region after 0800 UTC on 8 September. The quasi-stationary MCS stood over the same region until the following morning and then evolved eastward with the surface front. High surface rainfall was recorded over the Gard department, with a maximum of recorded daily precipitations that has reached about 700 mm. Figure 3 presents the accumulated rainfall from the Nîmes radar for the three phases of the rainfall event as identified by *Delrieu et al* [2005]: (1) during phase I (prior to 2200 UTC on 8 September, Figure 3a), the precipitation induced by the MCS were mainly over the plain region of the Gard department; (2) then phase II (between 2200 UTC on 8 September and 0400 UTC on 9 September, Figure 3b) was characterized by a shift of the MCS toward the upper regions at the limit of the mountain ridge (near Anduze), where it merged with the surface front that had progressed eastward during the same period; (3) during phase III (after 0400 UTC on 9 September, Figure 3c), the front with the embedded convection moved eastward and again swept over the Gard plain region. Figure 4 shows the temporal evolution of the hourly rainfall for two rain gauges; one (Anduze station) corresponds to the region where the maximum daily surface rainfall was recorded. The second one (Orange station) is situated 60 km eastward and north of the CHRN GPS station (see Figure 1 for locations). The Orange station recorded significant precipitation during phase I, then rainfall weakened when the precipitating system moved westward over the upper regions (phase II), before again showing rainfall peaks corresponding to the front passage (phase III). The temporal evolution of ZTD at CHRN station is well correlated with the precipitation evolution at Orange and also shows the three phases. At Anduze, significant rainfall occurred mainly from the end of phase I to the beginning of phase

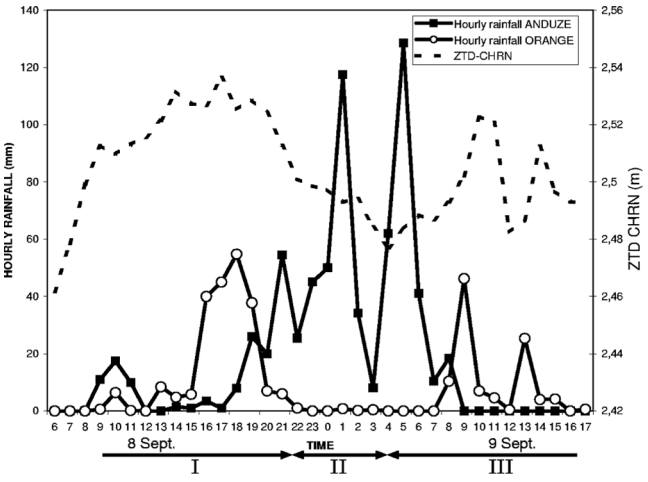

Figure 4. Temporal evolution from 0600 UTC on 8 September 2002 to 1800 UTC on 9 September 2002 of ZTD (m) at CHRN (dashed curve) and of hourly surface rainfall (mm) at Anduze (solid line with squares) and Orange (solid line with circles) rain gauge stations. The three phases (I, II, and III) of the rainfall event identified by *Delrieu et al.* [2005] are also indicated at the bottom of the figure.

III. In less than 9 hours, 500 mm were recorded at Anduze. No rainfall was observed after 0900 UTC on the 9 September, the front and associated convection had already evacuated the Anduze region.

2.3. Characteristics of the Méso-NH Simulations

[9] The 8–9 September event has been simulated with the nonhydrostatic Méso-NH model. A comprehensive description of this model is given by *Lafore et al.* [1998]. The simulations were performed using two nested grids (Figure 1) interacting with each other according to a two way interactive grid-nesting method [*Clark and Farley*, 1984; *Stein et al.*, 2000]. The horizontal resolution of the two domains are 9.5 and 2.4 km, respectively. In the following, only the delays and IWV for the 2.4-km domain are discussed. The vertical grid is defined by a stretched vertical coordinate [*Gal-Chen and Sommerville*, 1975], with 40 vertical levels spaced by 75 m in the lowest levels to 900 m at the top of the model which is at about 20 km. The prognostic variables are the three-dimensional wind components, the potential temperature, the mixing ratios of six water variables (vapor, cloud water, rainwater, primary ice, graupel, snow) and the turbulent kinetic energy. A bulk microphysical scheme [*Caniaux et al.*, 1994; *Pinty and Jabouille*, 1998] governs the equations of the six water species. Convection is explicitly resolved for the inner domain (no convective parameterization scheme).

[10] In this study, three experiments have been considered. The simulations differ only by their initial conditions [*Ducrocq et al.*, 2002; *Chancibault et al.*, 2006]. The first one (ARP12 experiment) starts from the analysis of the large-scale global ARPEGE system (ARPEGE for Research Project on Small and Large Scales, Météo-France NWP system). For the second one (RAD12 experiment), the mesoscale initialization procedure of *Ducrocq et al.* [2000] has been applied. It is composed of a mesoscale surface observation analysis and an adjustment of water vapor and hydrometeor contents based on the radar reflectivity and infrared Météosat brightness temperature valid for 8 September at 1200 UTC. The mesonet surface observations, which are on average spaced by about 30 km, are analyzed by an optimal interpolation analysis that has been tuned for the mesoscale [*Calas et al.*, 2000; *Ducrocq et al.*, 2000]. Then, a cloud and precipitation analysis based on the radar and satellite data updates the water vapor by imposing saturation inside cloudy regions, and adds rainwater[snow] below[above] the freezing level according to the reflectivity values. For the AMA12 experiment, the water vapor and hydrometeor adjustment is not applied; its initial state is simply obtained from the mesoscale surface data analysis. The background to the mesoscale initialization procedure is provided by the 1200 UTC ARPEGE analysis, so that the initial conditions of ARP12 and AMA12 differ only in the boundary layer, whereas middle and upper tropospheric moisture and hydrometeors are added inside the observed cloudy and rainy regions in the initial conditions of RAD12 with respect to AMA12. *Chancibault et al.* [2006] have performed a hydrological validation of these experiments and showed that high-resolution simulations improve the amount of surface rainfall compared to the actual operational models. In addition, the mesoscale initialization procedure improves significantly the location of the MCS during the phase I of the event.

2.4. Assessments of Zenith Delays and Integrated Water Vapor Content From Méso-NH Outputs

[11] Computation of zenith delays and IWV has been incorporated in the postprocessing of the Méso-NH model. The synthetic delays and IWV have been computed at each column of the 2.4 km domain, providing 2D fields of these parameters. An estimation of the synthetic delays at GPS station locations inside the Méso-NH domain has also been developed. For that purpose, a bilinear interpolation between the four closest grid columns is applied and the differences between the model orography and the true station altitude are also taken into account. For the eighteen GPS stations inside the inner Méso-NH domain (Figure 1b), only VERC is below the model orography of the 2.4-km domain, with a departure of only 25 m. All the other stations are above the model orography, with a maximum difference for AIGL (436 m). An altitude correction has to be considered (for GPS sites in mountainous regions essentially). However, such corrections are not straightforward, especially when extrapolation below the model orography is required. We have applied an altitude correction only when the real station height is above the model orography, by removing the contributions to the vertical integration below the height of the GPS sites. In our simulations, such corrections may induce a delay reduction of up to 13.5 cm for AIGL. No correction is proposed for the stations below the model orography in this study (only VERC is concerned). However, a correction can be considered for future work. Extrapolation methods such as the one proposed by *Vedel et al.* [2001] that assumes a hydrostatic state of the atmosphere, con-

stant relative humidity and a constant temperature lapse rate could be retained.

2.4.1. Retrieval of Zenith Delay

[12] The zenith total delay may be expressed as

$$\begin{aligned} \mathrm{ZTD} &= 10^{-6}\int_0^\infty \left(\mathrm{k_1 R_d}\rho_h + (\mathrm{k_2 R_w} - \mathrm{k_1 R_d})\rho_w + \mathrm{k_3}\frac{\mathrm{e}}{T^2}\right)\mathrm{dz} \\ &\quad + 10^{-6}\int_0^\infty (\mathrm{N}_{lw} + N_{ice})\mathrm{dz} \\ &= 10^{-6}\int_0^\infty \left(\mathrm{k_1}\frac{\mathrm{P}}{\mathrm{T}_v}\right)\mathrm{dz} + 10^{-6}\int_0^\infty \left(\mathrm{k'_2}\frac{\mathrm{e}}{\mathrm{T}} + \mathrm{k_3}\frac{\mathrm{e}}{\mathrm{T}^2}\right)\mathrm{dz} \\ &\quad + 10^{-6}\int_0^\infty (\mathrm{N}_{lw} + N_{ice})\mathrm{dz} \end{aligned} \quad (1)$$

where R_d = (287.0586 ± 0.0055) J/(kmol K) is the specific molar gas constant for dry air, R_w = (461.525 ± 0,013) J/(kmol K) the specific molar gas constant for water vapor, ρ_h, ρ_w are the densities of moist air and water vapor, P, e are the total pressure and the partial pressure of water vapor, T_v is the virtual temperature, $\mathrm{k_1}$, $\mathrm{k_2}$, $\mathrm{k_3}$ and $\mathrm{k'_2} = \mathrm{k_2} - \mathrm{k_1}\frac{\mathrm{R}_d}{\mathrm{R}_w}$ are refractivity coefficients, and N_{lw}, N_{ice} are respective contributions of liquid and ice water to refractivity. The first term after the second equals sign represents ZHD, the second term represents ZWD, and the third term represents zenith hydrometeors delay (ZHMD). For the Méso-NH model, mixing ratios of cloud and water rain are available for liquid water components, and mixing ratios of pristine ice, snow and graupel for ice water components.

[13] Zenith hydrostatic delay (ZHD) represents the contribution of the total atmospheric density to ZTD (including water vapor density). Zenith wet delay (ZWD) is the specific additional contribution of atmospheric water vapor to ZTD. The Méso-NH microphysics permits to describe five classes of hydrometeors. The zenith hydrometeors delay (ZHMD) depends on their total density. Appendix A presents the expressions of N_{lw} and N_{ice} which allow the assessment of the ZHMD contribution to ZTD. Note that the hydrostatic assumption has not been used to establish Zenith hydrostatic delay (ZHD) in equation (1), according to the Méso-NH equation system.

[14] In the case of the analysis of GPS data, the hydrostatic equilibrium is generally assumed so that ZHD can be evaluated from observations of surface pressure [*Saastamoinen*, 1972; *Davis et al.*, 1985]:

$$\mathrm{ZHD}_{\mathrm{P_S}} = 10^{-6}\frac{\mathrm{k_1 R_d P}_S}{\mathrm{g}_m} \quad (2)$$

where $\mathrm{k_1}$ can be fixed to a constant value (0.7760 ± 0.0005 K/Pa), P_S is the surface pressure and g_m is the gravity in the center of the atmospheric column following *Saastamoinen* [1972] ($g_m = 9.784 \times (1 - 0.0026\cos(2\lambda) - 0.000279\,\mathrm{H})$ with H the height of the GPS station and λ its latitude). When the model vertical column is in hydrostatic equilibrium, ZHD from equation (1) is reduced to equation (2), except that the gravity component in the center of the column g_m is replaced by the gravity used in the Méso-NH model (i.e., $g_0 = 9.807\ \mathrm{ms}^{-2}$).

[15] The Méso-NH model provides prognostic variables (pressure, temperature and mixing ratio) at the middle of its vertical layers. The vertical integration to estimate ZHD, ZWD and ZHMD is made up by the accumulation of each layer's contribution from ground surface to the uppermost layer in the model. Beyond the uppermost layer (i.e., $Z_{top} \approx 20$ km), the mixing ratio of water vapor is weak, as are the hydrometeor contents. Therefore neglecting the contribution of ZWD and ZHMD to ZTD above the uppermost layer of the model is legitimate. However, the contribution of ZHD outside the model ($\mathrm{ZHD}_{out} = \int_{Ztop}^{\infty}(\mathrm{k_1}\frac{\mathrm{P}}{\mathrm{T}_v})\ \mathrm{dz}$) cannot be neglected as it provides significant contributions up to an altitude of approximately 80 km [*Vedel et al.*, 2001]. The hydrostatic equilibrium can be assumed above the top of the model and thus ZHD_{out} is reduced to the hydrostatic formulation (equation (2)) using the pressure and the gravity acceleration at the top of the model.

2.4.2. Atmospheric Refractivity Coefficients

[16] Several sets of constants for the refractivity coefficients $\mathrm{k_1}$, $\mathrm{k_2}$, and $\mathrm{k_3}$ have been proposed in the literature [*Smith and Weintraub*, 1953; *Essen and Froome*, 1963; *Thayer*, 1974; *Hasegawa and Stokesberry*, 1975; *Bevis et al.*, 1994]. *Saastamoinen* [1973b] has proposed an expression of $\mathrm{k_1}$ as a function of $\mathrm{P_d}$ and T (see Appendix B). For this study, the expression $\mathrm{k_1(P_d, T)}$ has been adapted to GPS frequencies considering the wavelengths of approximately 19 cm (for $\mathrm{L_1}$), 24.4 cm (for $\mathrm{L_2}$), and 10.7 cm (for the ionosphere free linear combination used in the GPS analysis: $\mathrm{L_C}$), and considering dry air as a perfect gas:

$$\mathrm{k_1(P_d, T)} \approx \chi\left(1 + \beta\frac{\mathrm{P_d}}{\mathrm{T}}\right) \quad (3)$$

χ and β can be considered in good approximation as constant values for the given frequencies of the L band ($\mathrm{L_1}$, $\mathrm{L_2}$ or $\mathrm{L_C}$). We suggest $\chi = 0.7755$ K/Pa and $\beta = 1.3 \times 10^{-7}$ K/Pa. Constant values of $\mathrm{k_2}$ = (0.704 ± 0.022) K/Pa and $\mathrm{k_3}$ = (373900 ± 1200) $\mathrm{K^2/Pa}$ have been used [*Bevis et al.*, 1994].

2.4.3. ZTD-ZWD-IWV Relations

[17] Integrated water vapor retrieval from GPS data ($\mathrm{IWV_{GPS}}$) is commonly done by isolating zenith wet delays ($\mathrm{ZWD_{GPS}}$) from GPS-measured zenith total delays ($\mathrm{ZTD_{GPS}}$). For that, the zenith hydrostatic delay is assessed using surface pressure measurements ($\mathrm{ZHD_{P_S}}$, equation (2)), and then subtracted from $\mathrm{ZTD_{GPS}}$. The inferred ZWD is converted into IWV via a proportionality factor κ [*Hogg et al.*, 1981]:

$$\mathrm{IWV_{GPS}} = \kappa\ .\ \mathrm{ZWD_{GPS}} = \kappa\ .\ (\mathrm{ZTD_{GPS}} - \mathrm{ZHD_{P_S}}) \quad (4)$$

with ZWD in m, and IWV in $\mathrm{kg/m^2}$.

[18] The proportionality factor κ is a function of the atmospheric temperature profile [*Askne and Nordius*, 1987] (referred to as $\kappa_{A\&N}$ here after):

$$\kappa_{A\&N} \approx \frac{10^8}{\mathrm{R_w}\left(\frac{\mathrm{k_3}}{\mathrm{T}_m} + \mathrm{k'_2}\right)} \text{ with } \mathrm{T}_m = \frac{\int_L \frac{\mathrm{e}}{\mathrm{T}}\mathrm{dz}}{\int_L \frac{\mathrm{e}}{\mathrm{T}^2}\mathrm{dz}} \quad (5)$$

The Méso-NH model offers the possibility to compute directly the "true" integrated water vapor ($\mathrm{IWV_{Meso\text{-}NH}}$) by

vertical integration of the water vapor content (ρ_w) through the model vertical layers:

$$\mathrm{IWV}_{\mathrm{Meso-NH}} = \int_L \rho_w \mathrm{d}z \tag{6}$$

3. Sensitivity Tests on Zenith Delay Formulation

[19] In this section, the sensitivity of the zenith delay formulations to various factors (expression of refractivity coefficients, hydrometeor contributions, hydrostatic assumption, conversion of ZWD into IWV) is evaluated, based on the simulations of the 8–9 September 2002 event. To help synthesizing the results, statistical parameters have been computed (mean biases and standard deviations). They concern the calculation of delays and IWV, evaluated at each column within the model and at an hourly step between 1200 UTC, 8 September 2002, and 0600 UTC, 9 September 2002, resulting in a population of 240 × 240 × 18 elements. A reference for the delay formulations is defined (equation (1) with refractivity constants from *Bevis et al.* [1994] and no hydrometeor contributions) and the statistics aim at documenting the departures from this reference by a given sensitivity test. The statistical parameters are presented for the AMA12 simulation; results for the two other experiments (ARP12 and RAD12) do not differ significantly from AMA12 ones. When analyzing these statistical parameters, one must bear in mind that from a meteorological point of view, 6 millimeters of ZWD correspond approximately to 1 kg/m^2 of IWV which is the limit of resolution of standard meteorological water vapor measurements.

3.1. Refractivity Coefficients

[20] For a complete analysis of the sensitivity of the ZTD evaluation to the formulation of refractivity, different sets of refractivity constants k_1, k_2, k_3 proposed in the literature have been examined (two expressions of *Smith and Weintraub* [1953], two and three coefficients from *Essen and Froome* [1963], *Thayer* [1974], *Hasegawa and Stokesberry* [1975], and *Bevis et al.* [1994]). Our tests show that there are no significant differences in zenith delay evaluations between each set of constants (a mean ZTD bias of less than 2 mm and a maximum difference of less than 3.5 mm) except for the expression of ZTD from *Smith and Weintraub* [1953] with only two refractivity coefficients which is commonly used in GPS applications. The mean bias reaches nearly 12 mm and the maximum bias is 12.6 mm (overestimation). The significant overestimation is due to the approximation which has been made in obtaining one coefficient rather than two to formulate the water vapor contribution to the refractivity. The refractivity constants are given with uncertainties by the different authors. Considering the upper bounds of the uncertainty range leads to average biases of 2 mm for the *Bevis et al.* [1994] constants. Note that the ZTD estimates with different sets of refractivity constants are all included in the uncertainty range of *Bevis et al.* [1994] estimations, except for the two constants expression of *Smith and Weintraub* [1953].

[21] Figure 5 presents the temporal evolutions of ZHD and ZTD at CHRN station for $k_1(P_d, T)$ given by equation (3) and the *Bevis et al.* [1994] set of constants based on the RAD12 experiment. Departures between the use of a constant value of k_1 and the expression $k_1(P_d, T)$ reach at most 5 mm. The statistical parameters computed on the AMA12 experiment (Table 1, column 2) show that the mean bias is approximately 2 mm, for a maximum departure of 5 mm (6 mm for RAD12 and 5 mm for ARP12).

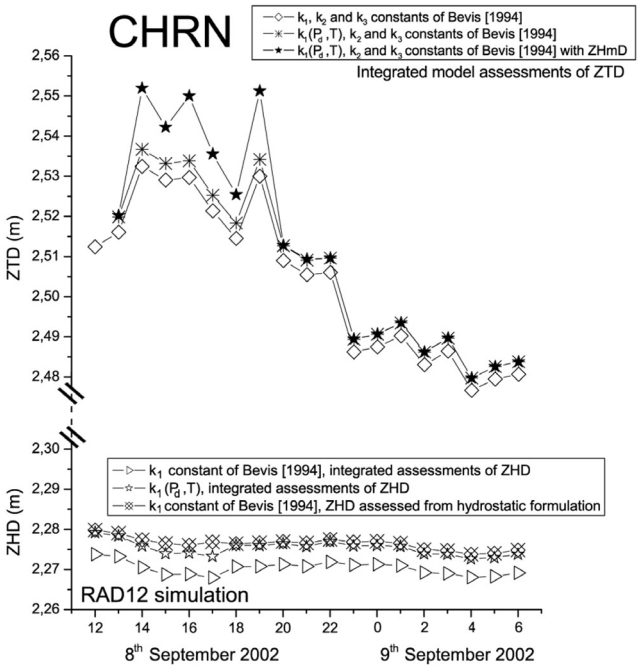

Figure 5. Time series of zenith delays (in m) estimated from different formulations at the CHRN GPS site the 8–9 September 2002 for the RAD12 experiment. The y axis has been cut to show ZTD and ZHD on the same graph keeping the same scale. At the top of this graph the zenith total delay is evaluated following equation (1): (1) with constant refractivity coefficients k_1, k_2, and k_3 from *Bevis et al.* [1994], (2) with a refractivity coefficient $k_1(P_d, T)$ from equation (3) and k_2, k_3 from *Bevis et al.* [1994], and (3) with $k_1(P_d, T)$ from equation (3), k_2, k_3 from *Bevis et al.* [1994], and contributions of hydrometeors to zenith delays (ZHMD) added. In the bottom part, ZHD has been evaluated: (1) from equation (1) with constant coefficients k_1 of *Bevis et al.* [1994], (2) from equation (1) with $k_1(P_d, T)$ following equation (3), and (3) from the hydrostatic formulation given by equation (2) and k_1 from *Bevis et al.* [1994].

[22] To sum up, results show a weak sensitivity to the refractivity coefficients, with differences in the domain of uncertainty of the water vapor measurements. In the following, $k_1(P_d, T)$, k_2 and k_3 of *Bevis et al.* [1994] are used.

3.2. Hydrostatic Formulation Versus Nonhydrostatic Formulation of ZHD

[23] ZHD is computed by vertical integration through the model grid thermodynamic profiles (equation (1)). It is compared with the commonly used formulation of ZHD deduced from ground pressure data (ZHD_{P_s}, equation (2)). These formulations of ZHD differ in two aspects: the gravity constant and the hydrostatic assumption. On the one hand, assuming an hydrostatic state, ZHD from equa-

Table 1. Statistical Results for ZHD From AMA12 Simulation[a]

	$k_1(P_d, T)$	ZHD_{P_S} with g_m	ZHD_{P_S} with g_0
Δ_{ZHD}^{mean} (mm)	2.1	6.0	−0.8
δ_{ZHD} (mm)	0.5	0.6	3.4
$\Delta_{ZHD_{min}}$ (mm)	−0.5	1.5	−3.7
$\Delta_{ZHD_{max}}$ (mm)	5.0	24.6	18.0

[a]The second column shows ZHD from equation (1) with $k_1(P_d, T)$ given by equation (3). The third column shows ZHD_{P_S} from equation (2), with g_m from *Saastamoinen* [1972]. The fourth column shows ZHD_{P_S} from equation (2), but with g_m replaced by g_0. The mean bias (Δ_{ZHD}^{mean}), the standard deviation (δ_{ZHD}), and the minimum and maximum departures ($\Delta_{ZHD_{min}}$ and $\Delta_{ZHD_{max}}$) are evaluated using as reference ZHD from equation (1) with the *Bevis et al.* [1994] constants set. The statistics consider the 18 hours of simulations and the 240 × 240 grid points.

tion (2) scales by g_m/g_0 the vertical integrated ZHD value. On the other hand, the nonhydrostatic equation system of Méso-NH allows us to fully study the impact of using or not an assumed hydrostatic equilibrium. Given the same gravity constant, it is therefore possible to isolate this impact of using an assumed hydrostatic equilibrium. For the heavy precipitation event simulated, the atmosphere departs from the hydrostatic equilibrium inside the vigorous deep convective cells as well as, to a lesser extent, within the gravity waves induced by the convection. The difference between the two formulations of ZHD (assuming the same gravity constant) is shown at 1500 UTC, 8 September 2002, on Figure 6a. Figure 6b presents the model reflectivity at the same time; only high values of reflectivity are shown in order to highlight the convective part of the rainfall system. Inside the intense convective cells (i.e., areas with reflectivity above about 40 dbZ), the pressure tends to be weaker than the hydrostatic pressure, resulting in larger delays for the hydrostatic formulation than for the integrated model one. The maximum difference of ZHD reaches 18 mm at 1500 UTC. The pressure is also larger than the hydrostatic pressure in some locations affected by gravity waves, leading to weaker delays for the hydrostatic formulation than for the integrated model one. The absolute values of the departure from the hydrostatic equilibrium are however weaker than inside the convective cells.

[24] Figure 5 displays the temporal evolution of ZHD at the CHRN station (bottom part of the graph) for the hydrostatic formulation including two sources of differences (i.e., gravity constant and hydrostatic assumption) from the model integrated estimation (equation (1)). The ratio between g_m and g_0 is about 0.997 for the CHRN station, which leads to a mean shift between the ZHD_{P_S} curve and the model integrated ZHD one of about 6 mm, except between 1400 and 1700 UTC on 8 September 2002 where the departure is slightly larger. Indeed, between 1400 and 1700 UTC, 8 September 2002, the Méso-NH model simulates convective cells in the region of CHRN, leading to nonhydrostatic vertical profiles at CHRN. Therefore, for that period, the departure between ZHD_{P_S} and the model integrated ZHD is increased, reaching 9 mm. The statistical parameters confirm the overestimation by the hydrostatic formulation. Table 1 presents statistical results for both sources. Column 3 evaluates the differences between the hydrostatic formulation with a gravity constant defined by g_m [*Saastamoinen*, 1972] and the integrated formulation of ZHD in Méso-NH. The mean departure is about 6 mm. Column 4 evaluates the differences using g_0 for the hydrostatic formulation, thus isolating the impact of the hydrostatic assumption. The departures due to the hydrostatic assumption range from −3.7 mm to 18 mm. This highlights potential errors in the estimation of ZWD and IWV extracted from GPS ZTD measurements inside observed convective systems. Using a constant gravity in ZHD computation allows to be consistent with the NWP model equations, but it induces a bias with respect to the estimation of ZHD using a more realistic variable g like the one proposed by *Saastamoinen* [1972](i.e., g_m). As a first approach, the bias can be corrected by scaling the model ZHD, by $\frac{g_m}{g_0}$ even though g_m is also based on assumptions derived from climatology which may be not valid for such extreme situations as the one considered here.

3.3. Hydrometeor Contributions to Zenith Delay (ZHMD)

[25] In this section, the contributions of liquid water and icy hydrometeors to zenith delays (ZHMD) are estimated. Figure 5 (upper plot) shows the ZTD at the CHRN station including the ZHMD. It can be seen that ZHMD can reach more than 20 mm in the afternoon of 8 September 2002. These large contributions are mainly located inside the convective part of the MCS as can be seen on Figure 7 which displays ZHMD at 2100 UTC on 8 September 2002. ZHMD reaches more than 50 mm in the heart of the convective part of the simulated precipitation system which is materialized by the synthetic reflectivities displayed on Figure 7b. During the 18 hours of simulation, the maximum of ZHMD attains 70 mm at 1500 UTC 8 September. The contributions induced by liquid water species are generally 10 times larger than the icy species ones.

[26] Figure 8 shows the temporal evolution of the surface in the model concerned with significant hydrometeor contributions, splitting in four classes (5–10 mm, 10–15 mm, 15–20 mm and >20mm). Clearly the areas concerned by large ZHMD contributions are correlated with the convective activity of the system. Between 1400 and 1800 UTC, 8 September 2002, and after 0300 UTC, 9 September 2002, the surface with ZHMD contributions larger than 20 mm reach more than 1000 km^2. A surface of about 5000 km^2 is concerned by ZHMD contributions larger than 10 mm during the afternoon of 8 September. Therefore, for such torrential rain event, the hydrometeor contributions are far from being negligible.

3.4. Relationship Between ZWD and IWV

[27] Several authors have proposed to approximate κ by a linear function of the surface temperature, which is more attractive for GPS analyses as only observations of surface temperature are required instead of vertical temperature profile observations (see section 2.4.3 for the definition of κ and the formulation of $\kappa_{A\&N}$). *Bevis et al.* [1992] established such a relation depending on surface temperature from a global climatology of radiosoundings (referred to as κ_{Bevis}), while *Emardson and Derks* [1999] determined site- and region-dependent relations taking into account more than 120000 radiosoundings from 38 sites in

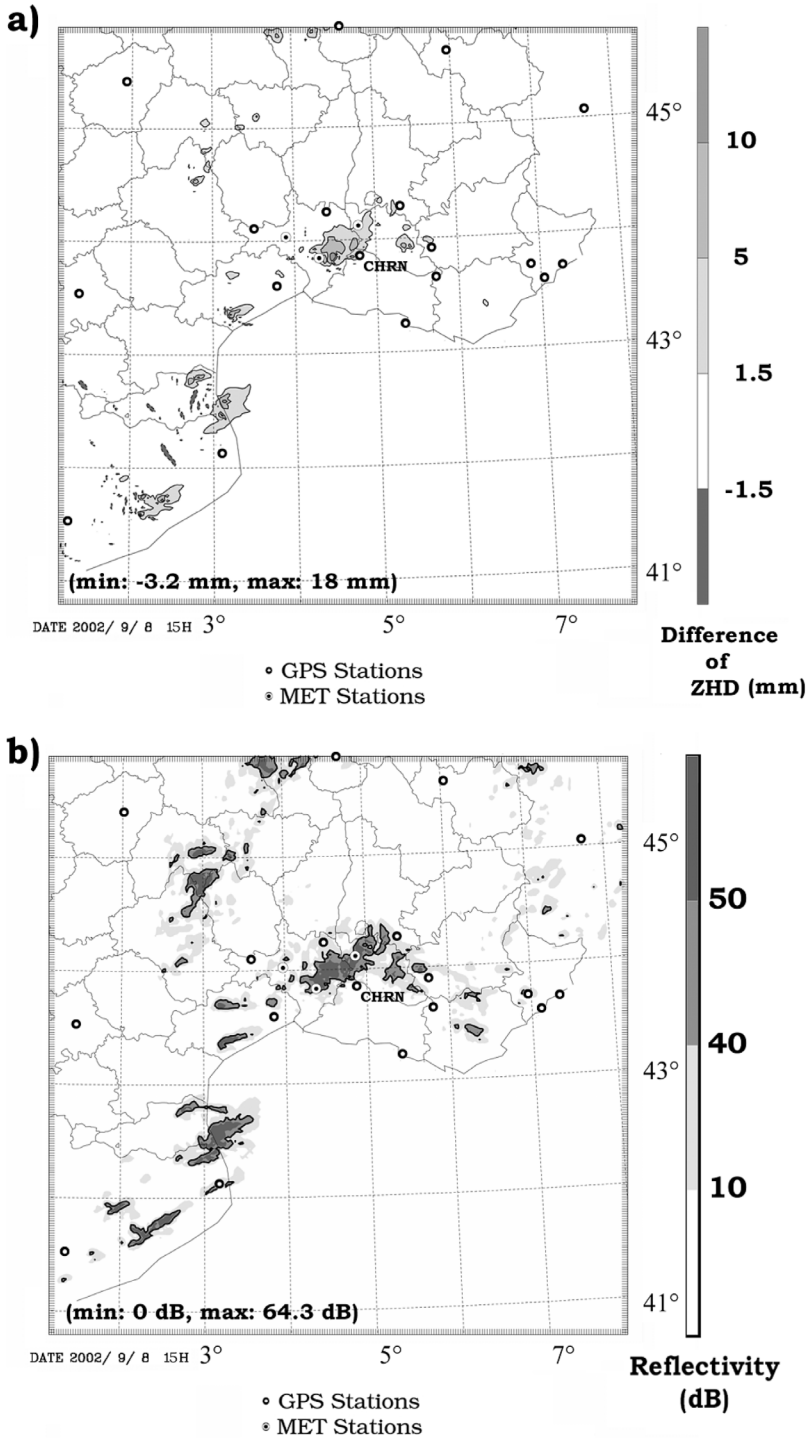

Figure 6. (a) Zenith hydrostatic delay (ZHD) difference (in mm) between the hydrostatic formulation following equation (2) but using g_0 and the integrated model formulation given by equation (1) at 1500 UTC on 8 September 2002 for the AMA12 experiment. (b) Model reflectivity for the same time and experiment (in dBZ, thick lines for the 40 dBz contour).

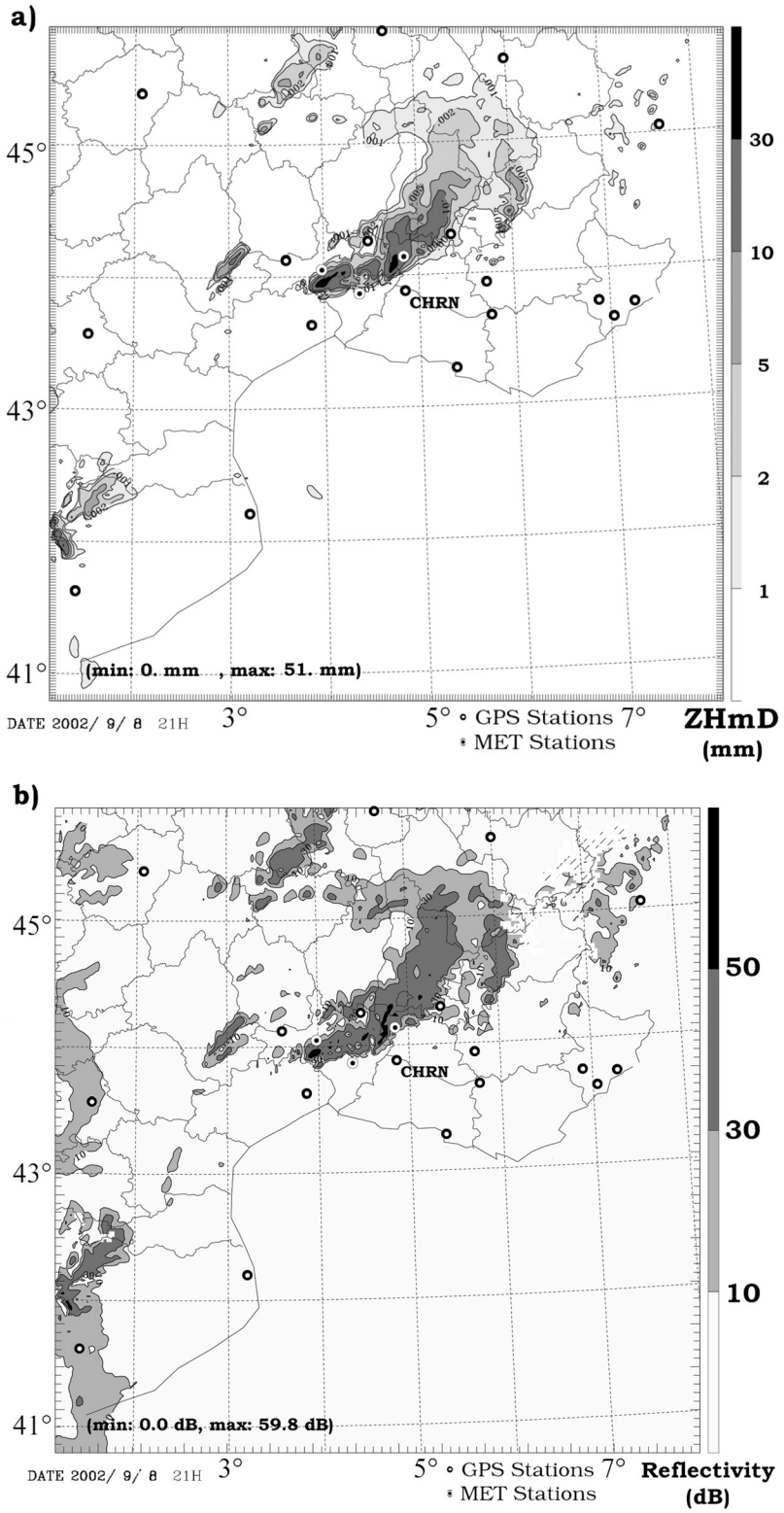

Figure 7. (a) Zenith hydrometeor delay (ZHMD in mm) evaluated at 2100 UTC on 8 September 2002 for the AMA12 experiment. (b) Synthetic radar reflectivity evaluated for the same experiment at the same time.

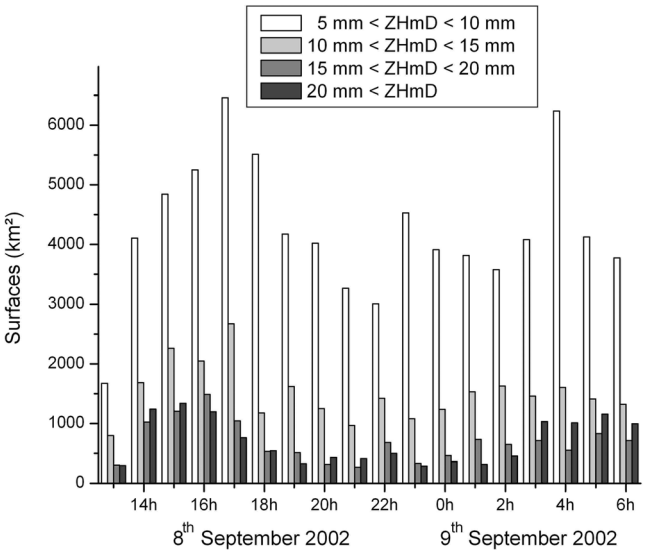

Figure 8. Temporal evolution of the surfaces concerned by ZHMD hydrometeor contributions ranking in four classes (5–10 mm, 10–15 mm, 15–20 mm, and >20 mm) from the RAD12 simulation.

Europe, with among them a specific relation for the Mediterranean region which is our region of interest (referred to as $\kappa_{E\&D}$):

$$\kappa_{Bevis} \approx \frac{10^8}{R_w\left(\frac{k_3}{T_m} + k_2'\right)} \text{ with } T_m \approx 70.2 + 0.72\ T_S \qquad (7)$$

$$\kappa_{E\&D} \approx \frac{10^3}{6.324 - 0.0177(T_S - 289.76) + 0.000075(T_S - 289.76)^2} \qquad (8)$$

We now examine the differences between, on the one hand, IWV deduced from model ZWD and applying $\kappa_{A\&N}$, κ_{Bevis} or $\kappa_{E\&D}$ as defined by equations (5), (7) and (8), and, on the other hand, from the model value of integrated water vapor ($IWV_{Meso\text{-}NH}$). The three first lines of Table 2 display the mean bias, the standard deviation as well as the maximum and minimum differences between the different IWV estimations with $\kappa_{A\&N}$, κ_{Bevis} or $\kappa_{E\&D}$ and $IWV_{Meso\text{-}NH}$. IWV obtained by the conversion with the κ given by *Askne and Nordius* [1987] corresponds almost exactly to $IWV_{Meso\text{-}NH}$. Figures 9a and 9b show the differences between $IWV_{Meso\text{-}NH}$ and $IWV_{\kappa_{Bevis}}$, and between $IWV_{Meso\text{-}NH}$ and $IWV_{\kappa_{E\&D}}$, respectively, *i.e.* the two formulations depending on surface temperature. Figure 9c presents the model $IWV_{Meso\text{-}NH}$. These values are calculated for the AMA12 experiment at 1500 UTC on 8 September 2002. $IWV_{Meso\text{-}NH}$ reaches more than 45 kg/m^2, implying $ZWD_{Meso\text{-}NH}$ values of more than 300 mm in the Gard region. We can see weaker values over the relief, and a moist area over the Mediterranean Sea and its littoral feeding the convective system. Figure 9a considers κ calculated with the expression of T_m (T_S) given by *Bevis et al.* [1992] based on a global climatology. It exhibits a highly variable differential field

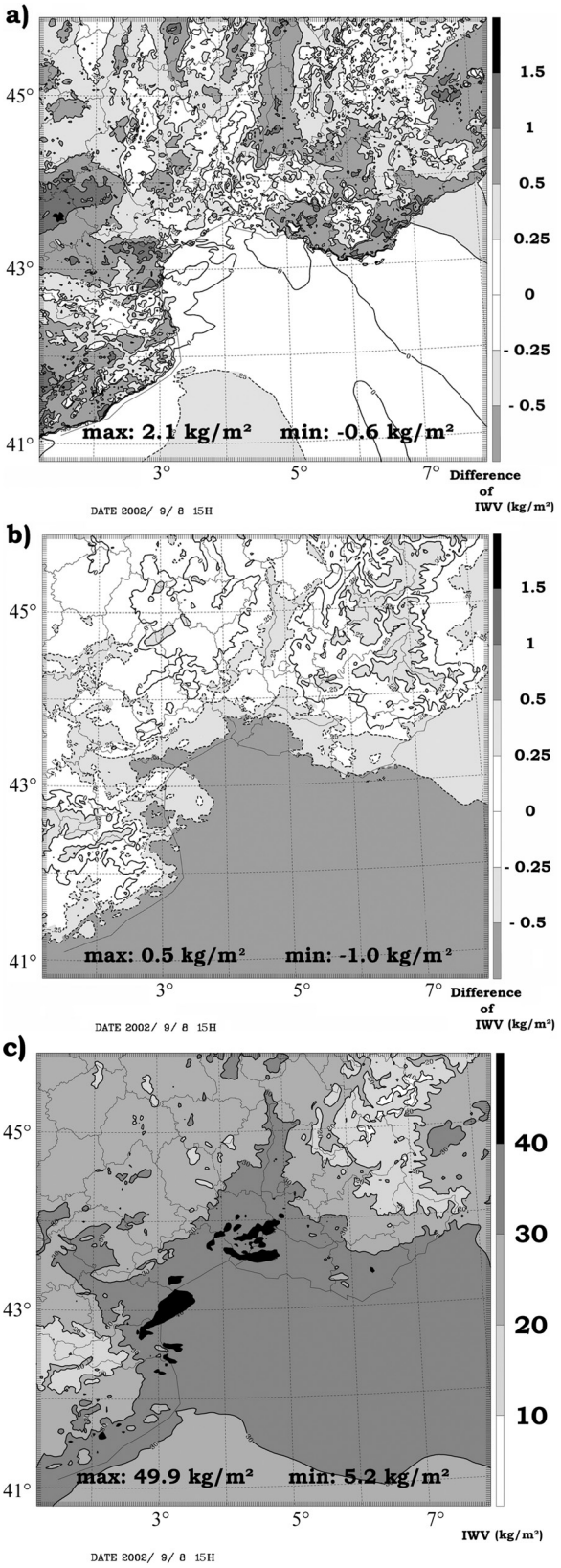

Figure 9. Differences between IWV conversions from ZWD and $IWV_{Meso\text{-}NH}$ (in kg/m^2) at 1500 UTC the 8 September 2002 from AMA12 experiment. (a) Difference between IWV (deduced from synthetic ZWD and κ_{Bevis}) and $IWV_{Meso\text{-}NH}$. (b) Same as Figure 9a but for $\kappa_{E\&D}$. (c) $IWV_{Meso\text{-}NH}$.

Table 2. Statistical Results of Different Methods of Conversions of ZWD Into IWV or Standard (GPS Stand-Alone) Extractions of IWV From ZWD (via ZHD Estimated From Ground Pressure)[a]

Type of Conversion	Δ_{IWV}^{mean}	$\Delta_{IWV_{max}}$	$\Delta_{IWV_{min}}$	δ_{IWV}
ZWD $\xrightarrow[\kappa_{Bevis}]{\kappa_{A\&N}}$ IWV	0.000	0.001	−0.001	0.000
ZWD $\xrightarrow[\kappa_{E\&D}]{\kappa_{Bevis}}$ IWV	0.076	2.056	−0.590	0.239
ZWD $\xrightarrow{}$ IWV	−0.240	0.517	−1.044	0.329
(ZWD + ZHMD) $\xrightarrow[\kappa_{E\&D}]{\kappa_{Bevis}}$ IWV	−0.144	11.385	−0.591	0.391
(ZWD + ZHMD) $\xrightarrow{}$ IWV	−0.171	10.776	−1.044	0.472
ZWD_{GPS} (with ZHMD) $\xrightarrow[\kappa_{E\&D}]{\kappa_{Bevis}}$ IWV	−0.202	8.309	−1.821	0.383
ZWD_{GPS} (with ZHMD) $\xrightarrow{}$ IWV	−0.513	7.730	−1.921	0.438
ZWD_{GPS} (without ZHMD) $\xrightarrow[\kappa_{E\&D}]{\kappa_{Bevis}}$ IWV	−0.271	2.084	−3.110	0.274
ZWD_{GPS} (without ZHMD) $\xrightarrow{}$ IWV	−0.582	0.384	−3.577	0.317

[a]Statistics have been computed for the AMA12 experiment, with the set of refractivity constants of *Bevis et al.* [1994]. Estimation of the mean difference Δ_{IWV}^{mean} and the standard deviations δ_{IWV} between deduced IWV and model IWV has been performed. The maximum positive and negative ($\Delta_{IWV_{max}}$ and $\Delta_{IWV_{min}}$) shifts are also presented. Values are in in kg/m^2.

covering an amplitude of 2.7 kg/m^2. The high variability of this field may arise from surface temperature variability induced by orography and land cover. Over the sea, the smoother surface temperature and the zero orography result in a smoother differential field. The mean difference is about 0.08 kg/m^2 (Table 2), whereas the maximum positive shift reaches 2 kg/m^2 and the maximum negative shift −0.6 kg/m^2. Figure 9b considers κ calculated with the expression of *Emardson and Derks* [1999], a Mediterranean specific climatology. With respect to the conversion with κ_{Bevis}, this one provides a smoother differential field with lower amplitudes of the variations (an interval of 1.5 kg/m^2 is covered). The conversion over the continental area yields IWV values close to $IWV_{Meso\text{-}NH}$. However, over almost all the sea surface, the differences of the IWV evaluations reach more than −0.5 kg/m^2. This results in a mean bias of −0.24 kg/m^2 (higher than that of Bevis et al.), but the maximum positive shift reaches only 0.45 kg/m^2 and the maximum negative shift only −0.86 kg/m^2 (lower than that of Bevis et al.). The ZWD to IWV conversion formula of *Emardson and Derks* [1999] appears more adapted to our study than the one of *Bevis et al.* [1992]. However, the comparison of these two conversions show very weak differences in IWV. Only sparse sites present more than 1 kg/m^2 of IWV differences between the *Bevis et al.* [1992] and the *Emardson and Derks* [1999] conversion, without correlation with the location of the IWV maximum.

[28] In rows 4 and 5 of Table 2, the conversion of the sum of ZWD and ZHMD into IWV has been estimated, simulating the fact that in GPS stand-alone IWV measurements ZWD and ZHMD cannot be distinguished. The statistical results show mean biases of less than 0.2 kg/m^2, but the extreme values reach more than 10 kg/m^2. That means there is a risk of bad conversion of ZWD into IWV with κ inside intense precipitation systems when a distinction between ZWD and ZHMD is not available, as is generally the case for GPS measurements of IWV.

[29] The different error sources of the standard GPS IWV extraction are now compared in more detail. Model estimated ZTD has been reduced by ZHD_{P_S} determined from ground pressure to ZWD, then the extracted ZWD is converted into IWV by κ_{Bevis} or $\kappa_{E\&D}$. Four more statistical results concerning this standard GPS IWV extraction are presented in Table 2 (rows 6–9). Model ZTD is always the sum of ZWD, ZHMD and ZHD. In rows 6 and 7, IWV extractions from (for GPS stand-alone measurements inseparable) ZWD + ZHMD contributions are estimated (IWV = κ (ZWD + ZHMD)). Extraction with κ_{Bevis} and $\kappa_{E\&D}$ are quasi equivalent: the mean biases are less than 0.6 kg/m^2. This degradation with regard to rows 4 and 5 is due to the ZHD determination from P_S with the hydrostatic formulation. However, as for rows 4 and 5 of Table 2, including hydrometeor contributions in the IWV conversion induces high extreme values of the differences with respect to model IWV (close to 8 kg/m^2). This lower value with respect to the approximately 11 kg/m^2 in rows 4 and 5 (where integrated ZHD was used to separate ZWD from ZTD) is due to the overestimation of ZHD and the subsequent underestimation of ZWD by the hydrostatic formulation. In rows 8 and 9, IWV extractions from ZWD without ZHMD contribution (IWV = κ ZWD) are proposed. Information about ZHMD necessary to separate it from GPS deduced ZWD as suggested in this test could be provided by polarimetric radar measurements. The mean biases are similar to the previous values in lines 6 and 7, but the extreme values are limited to a little more than 3 kg/m^2.

[30] The determination of IWV from GPS ZTD is sufficiently precise in average to yield significant observations for the assimilation of IWV_{GPS} in NWP, considering that 1 kg/m^2 of IWV is the limit of resolution of standard meteorological water vapor measurements. All mean differences of the different retrieval strategies with respect to model IWV presented in Table 2 are below 0.6 kg/m^2. The larger part of these differences in the estimation of IWV from GPS-like strategy is due to the ZHD approximation with the hydrostatic formulation, not to the ZWD to IWV conversion with $\kappa(T_S)$. Special attention has to be paid in strong precipitation areas as large contributions to the delay due to the hydrometeors may be included in the GPS deduced ZWD.

4. Validation of the Méso-NH Simulations With GPS ZTD

[31] In this section, the zenith delays simulated by the three numerical experiments (ARP12, RAD12 and AMA12) are compared with the observed GPS ZTDs. This will allow us to quantify the impact of the three different initial

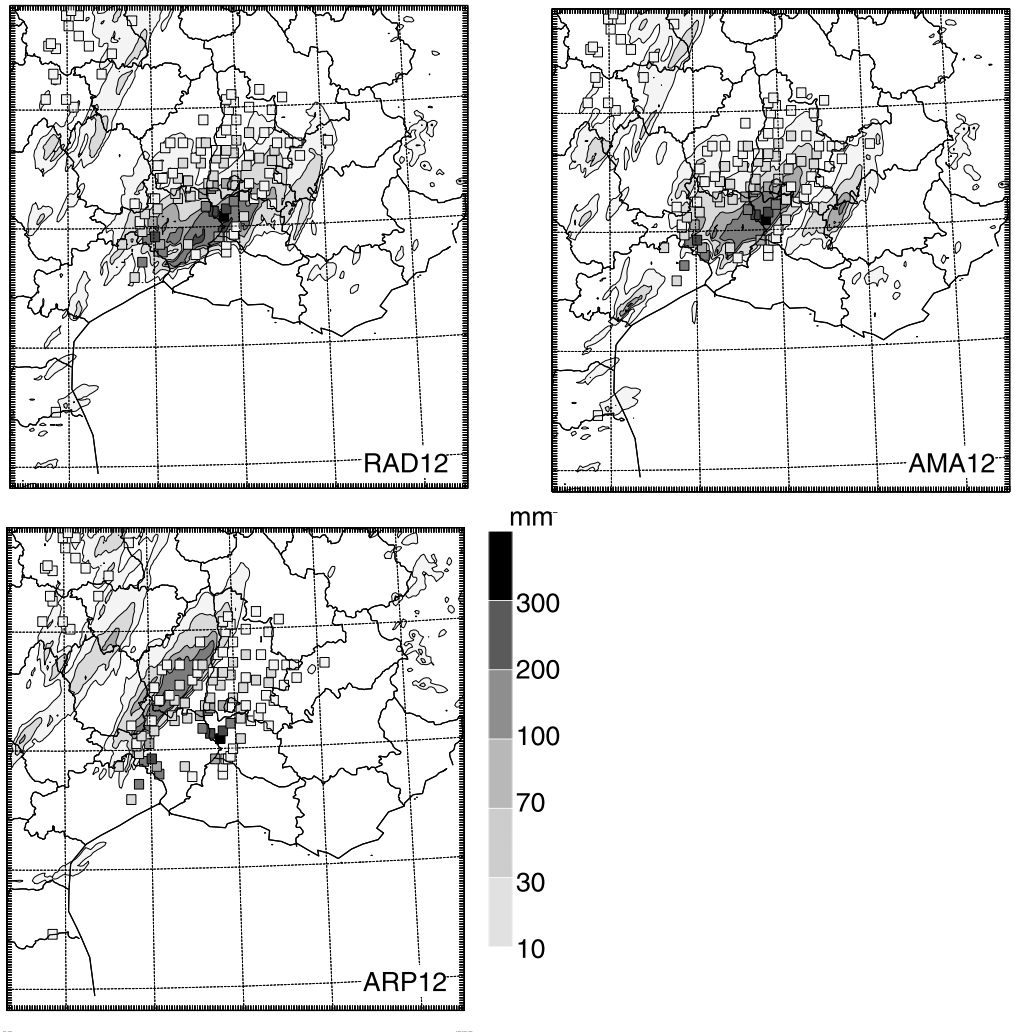

Figure 10. Accumulated rainfall (in mm, gray scale) for phase I (from 1200 to 2200 UTC, 8 September 2002) from the three Méso-NH simulations superimposed to the rain gauge data (gray boxes; only stations with accumulated rainfall larger than 10 mm are plotted).

conditions of the experiments on the delay estimation, and therefore on the value of integrated moisture throughout the troposphere. We will also verify that the simulation with the best fit to the GPS measurements is also the one simulating the best precipitation field. Figure 10 shows the accumulated surface rainfall during phase I of the event from the three numerical experiments, superimposed with the rain gauge data. When comparing to the rain gauge data and to the radar rainfall estimations (Figure 3a), the RAD12 and AMA12 simulations clearly provide a better localization of the heaviest precipitation during phase I of the event than the ARP12 simulation. RAD12 performs slightly better than AMA12 concerning the localization of the heaviest precipitation and the estimation of the maximum amount. An objective validation of these three simulations is given by *Chancibault et al.* [2006]. The observed and simulated mean areal rainfall depths have been compared for nine watersheds of the region. For the phase I, the relative error can reach 400% for the ARP12 simulation, whereas the relative error for RAD12 and AMA12 experiments never exceed a fifth of this value. Even though the differences in terms of relative error between RAD12 and AMA12 are weak, RAD12 performs in most cases better than AMA12, in particular for the Gard watersheds. For the two other phases of the event, the benefit of using a mesoscale data analysis as initial conditions decays; the three simulations have the same drawback which is an underestimation of rainfall over the Gard plain [*Chancibault et al.*, 2006].

[32] Figure 11 shows the ZTD assessments for the three simulations and observations at some of the GPS stations (see Figure 3 for locations). The GPS measurements are plotted from 0600 UTC on 8 September to 1700 UTC on 9 September, whereas the simulated ZTD are plotted from 1200 UTC on 8 September to 0600 UTC on 9 September. Note that GPS observations are missing at the MARS station at the end of the period. The mean differences between observed GPS ZTD and Méso-NH ZTD have been computed for all the GPS stations inside the 2.4 km domain, except for those too close to the borders of the model domain (mean scores, Figure 12). ZTD from simulations are

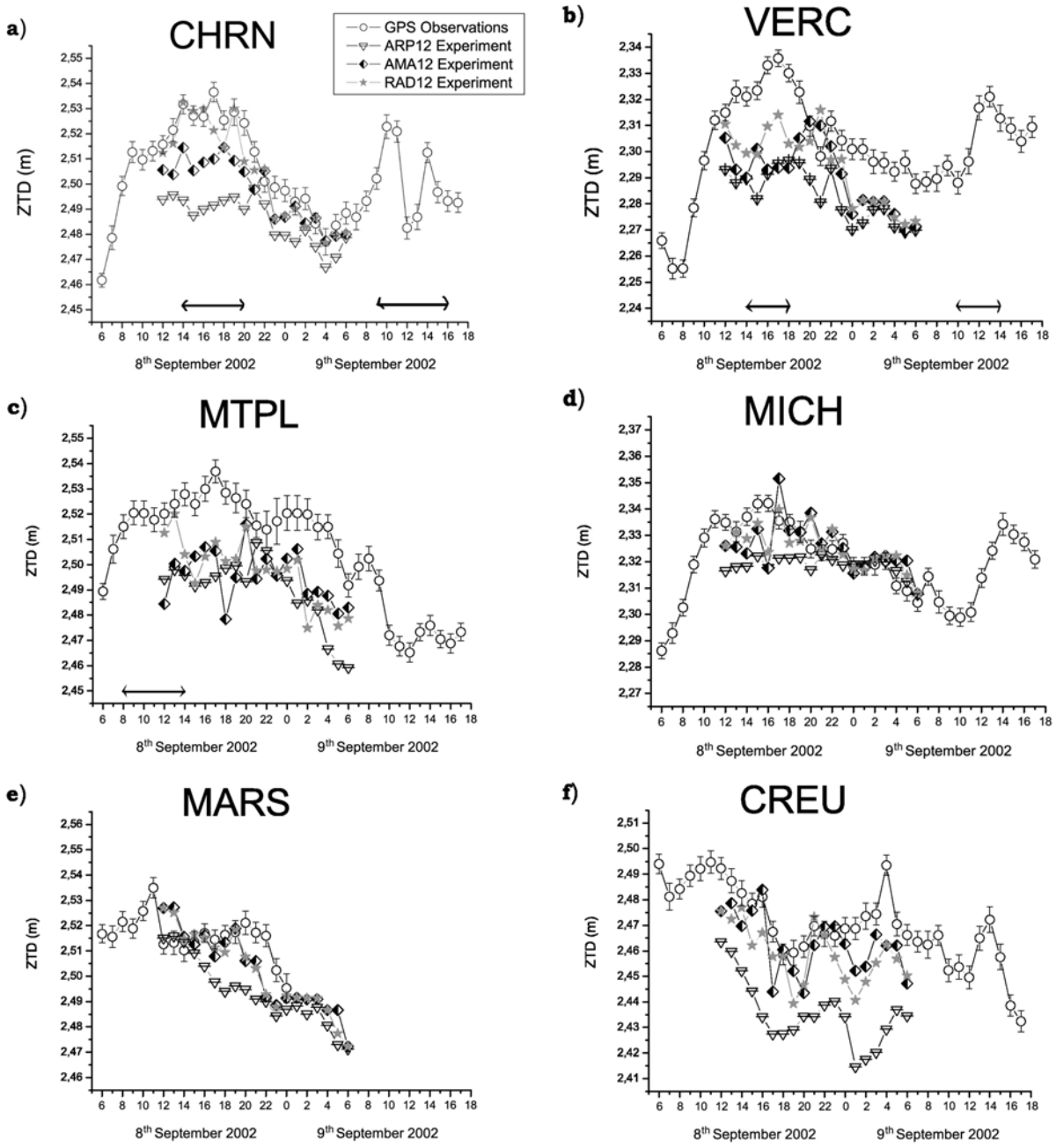

Figure 11. Time series (in m) at six GPS sites of ZTD observations and integrated assessments of synthetic ZTD with the set *Bevis et al.* [1994] of atmospheric refractivity coefficients considering three different experiments AMA12, ARP12, and RAD12. The error bars of GPS ZTD observations are formal errors evaluated by GAMIT. Double arrows along the time axis indicate the period of observed precipitation for the stations CHRN, VERC, and MTPL. No precipitation has been recorded for MICH, MARS and CREU.

based on equation (1) with *Bevis et al.* [1994] coefficients k_2 and k_3 and coefficient $k_1(P_d, T)$ from equation (3); the contributions from hydrometeors are included.

[33] The GPS sites of Chateau-Renard (CHRN) and Vercoiran (VERC) were affected by the convective precipitation during phase I of the event (before 2200 UTC on 8 September 2002; see Figure 3) and later during phase III with the passage of the front and the embedded convection (after 0400 UTC, 9 September 2002). Clearly, the two precipitating periods correspond to the highest observed ZTD values (Figures 11a and 11b). The observed ZTDs increase quickly in the morning of 8 September for the two stations (by 75–80 mm in less than 8 hours). Then, when the MCS moves toward the crests of the Massif Central

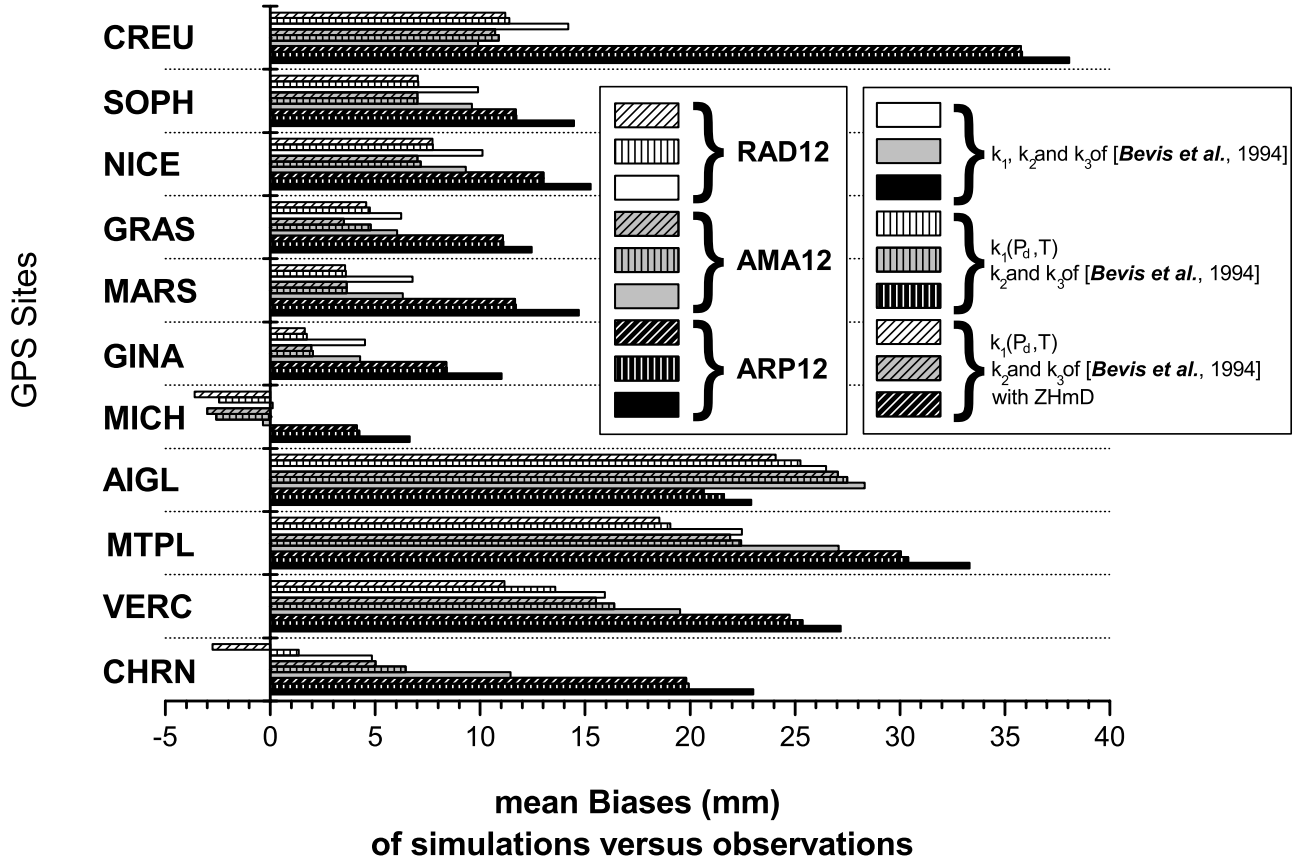

Figure 12. Biases (in mm) between the GPS ZTD observations and the simulated ZTD for the three Méso-NH experiments computed between 1200 UTC on 8 September to 0600 UTC on 9 September 2002. Black bars correspond to ARP12 experiment, gray bars correspond to AMA12, and white bars correspond to RAD12. A pattern of vertical lines corresponds to ZTD simulations with $k_1(P_d, T)$ and k_2 and k_3 of *Bevis et al.* [1994]. The additional contributions of hydrometeor (ZHMD) are presented with a pattern of slant lines. Plain bars correspond to ZTD simulations with k_1, k_2, and k_3 of *Bevis et al.* [1994].

(phase II of the event), the observed delays decrease before increasing again at the passage of the front with embedded convection. ZTDs computed from the ARP12 experiment show clearly an underestimation for the two stations during phase I of the event, which reduces slightly for the two subsequent phases. Using a mesoscale surface observation analysis as initial conditions (AMA12 experiment) improves the simulation of ZTD for VERC. However, clearly, adding to the surface observation analysis an adjustment of the moisture and hydrometeors based on radar and satellite data (RAD12 experiment) gives the best simulation of ZTD with a significant reduction of the bias for the two stations (Figure 12).

[34] In the western part of the network, heavy precipitation has been recorded only during the beginning of phase I at the Montpellier station (MTPL), whereas the Aigoual (AIGL) station was affected by heavy precipitation during phase II only (Figure 3). For these two stations, all simulations underestimate the ZTD values (Figure 11c for MTPL), with biases of more than 18 mm (Figure 12). This underestimation of ZTD cannot be explained by an underestimation of ZHD due to a bad forecast of surface pressure: differences between the GPS ZHD and the modelled ones are less than 6 mm. Therefore, the underestimation of ZTD for the three simulations are mainly linked to an underestimation in ZWD. So, the simulations starting from the mesoscale initial conditions do not succeed in improving the integrated water content of the atmosphere for the western stations.

[35] For the eastern sites, i.e., the stations of Ginasservis (GINA), St. Michel l'Observatoire (MICH), Marseille (MARS), Grasse (GRAS), Nice (NICE) and Sophia Antipolis (SOPH), no precipitation during the first two phases has been recorded (Figure 3). Again, the GPS observations show an increase of the ZTD values during the morning and beginning of the afternoon of 8 September, as it can be seen on the temporal evolution of ZTD for MICH and MARS (Figures 11d and 11e). However, the temporal increase is not as important as inside the heavy rain area, it does not exceed 30–50 mm. For all these sites, ARP12 underestimates the ZTD whereas the RAD12 and AMA12 experiments give systematically the best estimation of ZTD (Figure 12). RAD12 and AMA12 are close to the observations in the area of MARS, GINA and MICH (Biases < 5 mm). RAD12 and AMA12 ZTD values do not differ significantly. This is not astonishing as the adjustment added for RAD12 was introduced only over the observed rainy regions at 1200 UTC.

[36] The southern station, i.e., Cap de Creus (CREU) in Spain, was outside the region of the flood event; nevertheless, some convective cells have also passed over Cap de Creus during the studied period as for example at 0400 UTC on 9 September as evidenced by a peak in the observed ZTD time series (Figure 11f). As for the eastern stations, RAD12 and AMA12 significantly reduce the biases. ARP12 largely underestimate the observations with a bias of more than 35 mm.

[37] For the three experiments the use of $k_1(P_d, T)$ reduces the ZTD biases (except for MICH in the AMA12 and RAD12 experiments). This reduction is weak for high-altitude stations (AIGL and GRAS), but it reaches 5 mm for CHRN and MTPL. Hydrometeor contributions decrease the biases between observed and simulated ZTD (up to 3 mm of diminution for VERC), except for CHRN in the RAD12 experiment. The bias is 1.5 mm with $k_1(P_d, T)$ and becomes -3 mm with the additional ZHMD contribution. This highlights the fact that the contribution of hydrometeors is occasional in time and space, and that no time average has been taken into account in the model ZTD assessments. For this reason, we have simulated ZTD every 15 minutes for the RAD12 experiment, and calculated an average ZTD over one hour. The comparison of the averaged ZTDs to GPS observations presents a mean bias of -1 mm. When the contribution of ZHMD is very important a time average can be introduced in ZTD assessments to obtain more realistic simulations.

[38] For all the stations, whether or not taking into account the hydrometeor contributions or the $k_1(P_d, T)$ does not alter the superiority of RAD12 over the two other experiments. Clearly, RAD12 is the simulation that best fits the observed ZTD and consequently the integrated water vapor content of the troposphere inside the region covered by the convective system during phase I. This is also the simulation that best fits the rainfall observations. The ARP12 simulation, which gives the worst precipitation forecast, is the simulation that underestimates ZTD most (Figure 12). For phase II, when the system moves northwestward, the precipitation area does not extend southward enough in the simulations, even for the RAD12 experiment. Results at the GPS sites in this region clearly show an underestimation of ZTD for all the simulations during the afternoon and the night of 8–9 September.

5. Conclusion

[39] We used a high-resolution (2.4 km) nonhydrostatic atmospheric model (Méso-NH) to simulate GPS tropospheric observables during an extreme flash flood event that occurred the 8–9 September 2002 in southeastern France.

[40] Integrated evaluations of ZTD performed for the first time in such a high-resolution nonhydrostatic model permit us to quantify contributions of hydrometeors to zenith delays (up to 70 mm), and the extension of overestimations made by the hydrostatic formulation in ZHD evaluations inside strong convective cells (up to 18 mm). Several atmospheric refractivity coefficient sets proposed by the literature have been tested. Results show a weak sensitivity to the set chosen, except the one with only two coefficients from *Smith and Weintraub* [1953]. The use of a more precise pressure- and temperature-dependent expression for the refractivity coefficient $k_1 = k_1(P_d, T)$ yields ZTD differences from 1 to 6 mm.

[41] The comparison of the hydrostatic formulation of ZHD (its evaluation based on ground pressure measurements with the *Saastamoinen* [1972] formula) and an integrated reference evaluation shows differences related to two aspects, namely, (1) the use of two different terms for the gravity (g_m in the Saastamoinen formula, g_0 in the Méso-NH integration) which leads to an approximately 6 mm mean overestimation of ZHD by the hydrostatic evaluation from ground pressure and (2) the departure from hydrostatic equilibrium which induces an overestimation of up to 18 mm of ZHD by the evaluation based on ground pressure. These large differences are located inside the strong convective cells, where pressure departs from the hydrostatic equilibrium.

[42] The errors associated with ZWD conversions into IWV have been evaluated for ZWD inferred from ZTD using integrated ZHD and ZHD from ground pressure, and with or without separation of hydrometeor delay from ZWD. When using a conversion factor κ dependent on surface temperature, the κ given by *Emardson and Derks* [1999] shows the best performance in our study case. IWV from model-integrated ZWD converted by this $\kappa_{E\&D}$ has a low mean bias of 0.2 kg/m^2 with respect to model IWV and maximum differences of 1 kg/m^2. The mean bias between IWV from ZWD inferred using ZHD from ground pressure and model IWV yields 0.6 kg/m^2 with maximum differences of 8 kg/m^2. These large differences are locally confined and due to the ZHMD contribution contained in the value of ZWD. If ZHMD could be provided in an operational way inside the heavy rainfall areas, the maximum differences could be decreased to less than a quarter of the previous value. The increase of the mean IWV bias when using ZWD inferred by a GPS-like strategy using surface pressure and temperature is mainly due to the ZHD overestimation with the hydrostatic formulation, and less to the impact of ZHMD included in the ZWD. However, the unmodeled ZHMD contribution is responsible for the localized extreme differences inside the heavy rainfall event with respect to the model IWV field. Results on the impact of the hydrostatic assumption and of the hydrometeor contributions lead us to recommend caution when using IWV inferred from GPS ZTD inside vigorous convective and precipitating cells. Results show that the induced IWV error can reach 15% in the convective cells.

[43] The comparison of the three different model simulations with GPS observations of ZTD shows that the differences in simulated and observed ZTD are essentially due to underestimations of the wet delay and therefore to the water vapor content by the simulations. The simulation integrating the most precise information about the distribution of water vapor and water in the atmosphere obtains the best score (RAD12). Taking into account the contribution of ZHMD (more than 20% of the ZWD estimation in extreme cases) has a positive impact on the shape of the ZTD time series (up to 18% of bias diminution). The expression $k_1(P_d, T)$ present also a significant positif impact (up to 60% of bias diminution). The mesoscale network of GPS stations used for this study has allowed a detailed validation of the simulations. In particular, comparison with GPS ZTD for the western sites shows that all simulations suffer from an

underestimation of the delays, as well as for the CHRN and VERC stations during phases II and III of the event. The assimilation of these masoned GPS data is envisaged in the near future with the hope of improving the simulation of precipitation during phases II and III of the event. Our study favors assimilation of GPS ZTD measurements, rather than of GPS-inferred IWV, to avoid the significant errors due to hydrometeors and the ZHD overestimation made by the hydrostatic formulation in extreme weather situations.

Appendix A: Liquid Water and Ice Refractivity

[44] The propagation in the neutral atmosphere can be considered independent of the signal frequency (approximation with constant values for atmospheric refractivity coefficients). However, a contribution to neutral atmospheric refractivity can arise from some polar atmospheric gases [*Owens*, 1967] and hydrometeors [*Solheim et al.*, 1999]. In general, the total refractivity is expressed as $N(f) = N_0 + N'(f) + iN''(f)$, where N_0 and $N'(f)$ are the nondispersive and dispersive parts of refractivity related to the real part of the permittivity (phase of signal), and $N''(f)$ is dispersive attenuation, related to the imaginary part of the permittivity (amplitude of signal). However, in this study attenuation of the signal has not been considered ($N''(f) = 0$). Therefore only the delay induces by the neutral part of the atmosphere is considered. Influence of atmospheric carbon dioxide on refractivity has been studied by *Edlén* [1953, 1966], *Owens* [1967], and *Thayer* [1974]. In our work, we do not consider the influence of CO_2 on GPS signal propagation, because its atmospheric refractivity coefficient is badly constrained and the Méso-NH model does not provide any CO_2 information.

[45] However, dispersive propagation in the neutral part of atmosphere can be, among others, caused by particles formed by the condensation of water vapor (such as rain, hail, pristine ice, snow and graupel) [*Solheim et al.*, 1999; *Hajj et al.*, 2002]. Phase delays induced by these suspended forms of water can be approximated using calculations based on permittivity. A thin strip approximation for non gaseous and nonscattering particles and the Clausius-Mossoti equation for refractivity [*Debye*, 1929] can be applied in obtaining equation (A1) and equation (A4).

[46] *Liebe et al.* [1991] proposed, for a signal frequency less than 100 GHz, an approximate formulation (single Debye model) for the liquid water additional contribution to the real part of the refractivity (N_{lw}):

$$N_{lw} = \frac{3}{2} 10^6 \left[\frac{\varepsilon_{lw} - 1}{\varepsilon_{lw} + 2}\right] \frac{M_{lw}}{\rho_{lw}} \tag{A1}$$

where ρ_{lw} is the density of liquid water (≈ 1 g/cm^3), M_{lw} is the mass content of the liquid water particles per unit of air volume, and ε_{lw} is the permittivity of liquid water (function of T and f) defined as follows.

$$\varepsilon_{lw} = \varepsilon_s \left(1 - \frac{0.934}{1 + \left(\frac{f_D}{f}\right)^2}\right) \tag{A2}$$

where $\varepsilon_s = (77.66 - 103.3\ \theta)$ is the static dielectric coefficient, with $\theta = (1 - \frac{300}{T})$ and T the temperature expressed in K ($T \in [250-330]$); f is the microwave frequency in Hz and $f_D = (20.27 + 146.5\ \theta + 314\ \theta^2)10^9$ is the relaxation frequency in Hz. The specific refractivity contribution of liquid water to delay can be approximated by

$$N_{lw} \approx 1.45 \times 10^6\ M_{lw} \tag{A3}$$

Hufford [1991] proposed, for 1 MHz $\leq f \leq$ 1 THz, an approximate formulation for the ice additional contribution to the real part of the refractivity (N_{ice}):

$$N_{ice} = \frac{3}{2} 10^6 \left[\frac{\varepsilon_{ice} - 1}{\varepsilon_{ice} + 2}\right] \frac{M_{ice}}{\rho_{ice}} \tag{A4}$$

where ρ_{ice} is the density of ice (≈ 0.916 g/cm^3 [*Huining et al.*, 1999]), M_{ice} is the mass content of the solid water particles per unit of air volume, and $\varepsilon_{ice} = 3.185$ [*Mätzler*, 1996] the permittivity of ice. Specific refractivity contribution of ice to delay can be approximated by

$$N_{ice} \approx 0.69 \times 10^6\ M_{ice} \tag{A5}$$

These additional refractivity expressions for hydrometeors are an approximation to the mix formulae of *Garnett* [1904]. This formulation of delays caused by hydrometeors is valid for any medium considering inclusion of disjunct spherical particles (case of Méso-NH), with sizes of particles clearly smaller than the wavelength of the signal (case of hydrometeors size versus GPS wavelengths).

Appendix B: Refractivity Coefficient $k_1(P_d, T)$

[47] *Saastamoinen* [1973b] proposed an expression of k_1 as a function of P_d and T:

$$k_1(P_d, T) \approx \chi \left(1 + \beta \frac{P_d}{T} \frac{Z_{d_0}}{Z_d}\right) \frac{Z_{d_0}}{Z_d} \tag{B1}$$

where $\chi = \frac{(n_0-1)T_0}{P_{d_0}} \left(1 - \frac{(n_0-1)}{6}\right)$ and $\beta = \frac{(n_0-1)T_0}{6P_{d_0}}$, for temperature T_0, partial pressure of dry air P_{d_0}, compressibility factor of dry air Z_{d_0} and refractive index of dry air n_0 given in standard conditions, and compressibility factor of dry air Z_d at P_d and T [see *Owens*, 1967; *Birch and Downs*, 1993]. The ratio $\frac{Z_{d_0}}{Z_d}$ can be approximated by unity considering perfect gas. For the refractive index of air n_0, the correction to the updated Edlén equation is used [*Edlén*, 1966; *Birch and Downs*, 1994]:

$$n_0 = 1 + \left(8342.54 + 2406147\left(130 - \sigma^2\right)^{-1} + 15998\left(38.9 - \sigma^2\right)^{-1}\right)10^{-8} \tag{B2}$$

where σ is wave number in μm^{-1}. χ and β can be considered in a first good approximation like constant values. In fact, considering wavelengths of GPS (L band), in this expression of the refractive index of air n_0, we have actualized the expression of $k_1(P_d, T)$ derived by *Saastamoinen* [1973b] to GPS frequencies. These values are constant, independent of the GPS signal frequency (L_1, L_2 or L_C), but these

values are also constant because the proportion of dry air in the atmosphere is quasi-constant. For a wavelength of 0.574 μm [*Jordan et al.*, 1970], it gives the value of $\chi = 0.788828$ K/Pa and $\beta = 1.315 \times 10^{-7}$ K/Pa as suggested by *Saastamoinen* [1973b]. We suggest $\chi = 0.7754713$ K/Pa and $\beta = 1.2925 \times 10^{-7}$ K/Pa considering the L band (GPS frequency domain).

[48] **Acknowledgments.** The current study was performed under the PATOM and PNRH research programs of the CNRS-INSU (the National French Institute of Universe Sciences). This collaboration between the LGIT and the CNRM results from an ACI Ph.D. grant in the frame of the "Observatoire Hydrométéorologique Méditerranéen Cévennes-Vivarais" (OHM-CV). We thank Laurent Labatut for his informative management as well as Paddy O'Brien and Anne Holford for improving the English of the manuscript. We thank Paul Tregoning and two anonymous reviewers for their advice and their helpful contributions for improving this work.

References

Altamimi, Z., P. Sillard, and C. Boucher (2002), ITRF 2000: A new release of the International Terrestrial Reference Frame for Earth science applications, *J. Geophys. Res.*, *107*(B10), 2214, doi:10.1029/2001JB000561.

Askne, J., and H. Nordius (1987), Estimation of tropospheric delay for microwaves from surface weather data, *Radio Sci.*, *22*, 379–386.

Bean, B., and E. Dutton (1966), *Radio Meteorology*, 22 pp., Natl. Bur. of Stand., Washington, D. C.

Bevis, M., S. Businger, T. A. Herring, C. Rocken, R. A. Anthes, and R. H. Ware (1992), GPS meteorology: Remote sensing of atmospheric water vapor using the Global Positioning System, *J. Geophys. Res.*, *97*(D14), 15,787–15,801.

Bevis, M., S. Businger, S. Chiswell, T. Herring, R. A. Anthes, C. Rocken, and R. H. Ware (1994), GPS meteorology: Mapping zenith wet delays onto precipitable water, *J. Appl. Meteorol.*, *33*, 379–386.

Birch, K., and M. Downs (1993), An updated Edlén equation for the refractive index of air, *Meteorology*, *30*, 155–162.

Birch, K., and M. Downs (1994), Correction to the updated Edlén equation for the refractive index of air, *Metrology*, *31*, 315–316.

Bock, O., C. Keil, E. Richard, C. Flamant, and M.-N. Bouin (2005), Validation of precipitable water from ECMWF model analyses with GPS and radiosonde data during the MAP SOP, *Q. J. R. Meteorol. Soc.*, *131*, 1–24.

Boudouris, G. (1963), On the index of refraction of air, the absorption and dispersion of centimeter waves by gases, *J. Res. Natl. Bur. Stand., Sect. D*, *67*(6), 631–684.

Businger, S., S. Chiswell, M. Bevis, J. Duan, R. Anthes, C. Rocken, R. Ware, T. Van Hove, and F. Solheim (1996), The promise of GPS in atmospheric monitoring, *Bull. Am. Meteorol. Soc.*, *77*, 379–386.

Calas, C., V. Ducrocq, and S. Sénési (2000), Mesoscale analyses and diagnostic parameters for deep convection nowcasting, *Meteorol. Appl.*, *7*, 143–161.

Caniaux, G., J.-L. Redelsperger, and J.-P. Lafore (1994), A numerical study of the stratiform region of a fast-moving squall line, *J. Atmos. Sci.*, *51*, 2046–2074.

Champollion, C., F. Masson, J. Van Baelen, A. Walpersdorf, J. Chéry, and E. Doerflinger (2004), GPS monitoring of the tropospheric water vapour distribution and variation during the 9 September 2002 torrential precipitation episode in the Cévennes (southern France), *J. Geophys. Res.*, *109*, D24102, doi:10.1029/2004JD004897.

Chancibault, K., S. Anquetin, V. Ducrocq, and G.-M. Saulnier (2006), Hydrological evaluation of high resolution precipitation forecasts of the Gard flash-flood (8–9 September 2002), *Q. J. R. Meteorol. Soc.*, in press.

Clark, T., and R. Farley (1984), Severe downslope windstorm calculations in two and three spatial dimensions using anelastic interactive grid nesting: A possible mechanism for Gustines, *J. Atmos. Sci.*, *41*, 329–350.

Cucurull, L., B. Navascues, G. Ruffini, P. Elósegui, A. Rius, and J. Vil (2000), The use of GPS to validate NWP systems: The HIRLAM model, *J. Atmos. Oceanic Technol.*, *17*, 773–787.

Cucurull, L., J. Vil, and A. Rius (2002), Zenith total delay study of a mesoscale convective system: GPS observations and fine-scale modeling, *Tellus, Ser. A*, *54*, 138–147.

Davis, J. L., T. A. Herring, I. I. Shapiro, A. E. E. Rogers, and G. Elgered (1985), Geodesy by interferometry: Effects of atmospheric modeling errors on estimates of baseline length, *Radio Sci.*, *20*, 1593–1607.

Debye, P. (1929), *Polar Molecules*, Chem. Catalog Co., New York.

Delrieu, G., et al. (2005), The catastrophic flash-flood event of 8–9 September 2002 in the Gard region, France: A first case study for the Cévennes-Vivarais Mediterranean Hydrometeorological Observatory, *J. Hydrometeorol.*, *6*, 34–51.

Ducrocq, V., J. Lafore, J. Redelsperger, and F. Orain (2000), Initialisation of a fine scale model for convective system prediction: A case study, *Q. J. R. Meteorol. Soc.*, *126*, 3041–3065.

Ducrocq, V., D. Ricard, J. P. Lafore, and F. Orain (2002), Storm-scale numerical rainfall prediction for five precipitations events over France: On the importance of the initial humidity field, *Weather Forecast.*, *17*, 1236–1256.

Ducrocq, V., C. Lebeaupin, T. Thouvenin, H. Giordani, K. Chancibault, S. Anquetin, and G.-M. Saulnier (2004), The 8–9 September 2002 extreme flash-flood: Meteorological description and mesoscale simulations, *Houille Blanche*, *6*, 86–92.

Edlén, B. (1953), The dispersion of standard air, *J. Opt. Soc. Am.*, *43*(5), 339–344.

Edlén, B. (1966), The refractive index of air, *Metrologia*, *2*, 71–80.

Emardson, T. R., and H. J. P. Derks (1999), On the relation between the wet delay and the integrated precipitable water vapour in the European atmosphere, *Meteorol. Appl.*, *6*, 1–12.

Essen, L., and K. Froome (1963), 13th International Geodesy Association General Assembly, in *Bull. Geod.*, 70, 390 pp.

Gal-Chen, T., and R. Sommerville (1975), On the use of a coordinate transformation for the solution of the Navier-Stokes equations, *J. Comput. Phys.*, *17*, 209–228.

Garnett, J. M. (1904), Colours in metal glasses and in metallic films, *Philos. Trans. R. Soc. London*, *203*, 385–420.

Gendt, G., G. Dick, C. Reigber, M. Tomassini, Y. Liu, and M. Ramatschi (2004), Near real time GPS water vapor monitoring for numerical weather prediction in Germany, *J. Meteorol. Soc. Jpn.*, *82*, 370–391.

Hajj, G., E. Kursinski, L. Romans, W. Bertiger, and S. Leroy (2002), A technical description of atmospheric sounding by GPS occultation, *J. Atmos. Sol. Terr. Phys.*, *64*, 451–469.

Hasegawa, S., and D. Stokesberry (1975), Automatic digital microwave hygrometer, *Rev. Sci. Instrum.*, *46*, 867–873.

Herring, T. A., J. L. Davis, and I. I. Shapiro (1990), Geodesy by radio interferometry: The application of Kalman filtering to the analysis of very long baseline interferometry data, *J. Geophys. Res.*, *95*, 12,561–12,581.

Hogg, D. C., F. O. Guiraud, and M. T. Decker (1981), Measurement of excess transmission length on Earth-space paths, *Astron. Astrophys.*, *95*, 304–307.

Huet, P., X. Martin, J. Prime, P. Foin, C. Laurain, and P. Cannard (2003), Retour d'expérience des crues de Septembre 2002 dans les Départements du Gard, de l'Hérault, du Vaucluse, des Bouches du Rhône, de l'Ardèche et de la Drome, report, 133 pp, L'Inspection Gen. de l'Environ., Minist. de l'Ecol. et du Develop. Durable, Paris. (Available at http://www.ecologie.gouv.fr/IMG/pdf/crues_gard.pdf)

Hufford, G. (1991), A model for the complex permittivity of ice at frequencies below 1 THz, *Int. J. Infrared Millimeter Waves*, *12*(7), 677–682.

Huining, W., J. Pulliainen, and M. Hallikainen (1999), Effective permittivity of dry snow in the 18 to 90 GHz range, *Prog. Electromagn. Res.*, *24*, 119–138.

Jordan, W., O. Eggert, and M. Kneissl (1970), *Handbuch der Vermessungskunde*, vol. 2a, 107 pp., J. B. Metzler, Stuttgart, Germany.

King, R. W., and Y. Bock (2000), Documentation for the GAMIT GPS analysis software, version 10.07, Mass. Inst. of Technol., Cambridge.

Köpken, C. (2001), Validation of integrated water vapor from numerical models using ground-based GPS, SSM/I, and water vapor radiometer measurements, *J. Appl. Meteorol.*, *40*, 1105–1117.

Kursinski, E., G. Hajj, J. Schofield, R. Linfield, and K. Hardy (1997), Observing Earth's atmosphere with radio occultation measurements using the Global Positioning System, *J. Geophys. Res.*, *102*, 23,429–23,465.

Lafore, J., et al. (1998), The Meso-NH atmospheric simulation system. Part I: Adiabatic formulation and control simulations, *Ann. Geophys.*, *16*, 90–109.

Liebe, H., G. Hufford, and T. Manabe (1991), A model for the complex permittivity of water at frequencies below 1 THz, *Int. J. Infrared Millimeter Waves*, *12*(7), 659–675.

Liou, Y.-A., and C.-Y. Huang (2000), GPS observations of PW during the passage of a typhoon, *Earth Planets Space*, *52*, 709–712.

Masson, F., P. Collard, J. Chéry, E. Doerflinger, J.-F. Ritz, O. Bellier, D. Chardon, and M. Flouzat (2003), The VENICE Project: A GPS network to monitor the deformation of western Provence and eastern Languedoc (southern France), *Geophys. Res. Abstr.*, *5*, Abstact 04482.

Mätzler, C. (1996), Microwave permittivity of dry snow, *IEEE Tran. Geosci. Remote Sens.*, *34*(2), 573–581.

Niell, A., A. Coster, F. Solheim, V. Mendes, P. Toor, R. Langley, and C. Upham (2001), Comparison of measurements of atmospheric wet delay by radiosonde, water vapor radiometer, GPS, and VLBI, *J. Atmos. Oceanic Technol.*, *18*, 830–850.

Owens, J. C. (1967), Optical refractive index of air: Dependance on pressure, temperature and composition, *Appl. Opt.*, *6*, 51–58.

Pinty, J., and P. Jabouille (1998), A mixed-phased cloud parameterization for use in a mesoscale non-hydrostatic model: Simulations of a squall line and of orographic precipitation, paper presented at Conference on Cloud Physics, Am. Meteorol. Soc., Everett, Wash.

Rocken, C., R. Ware, T. V. Hove, F. Solheim, C. Alber, J. Johnson, M. Bevis, and S. Businger (1993), Sensing atmospheric water vapor with the Global Positioning System, *Geophys. Res. Lett.*, *20*, 2631–2634.

Rocken, C., T. V. Hove, J. Johnson, F. Solheim, R. Ware, M. Bevis, S. Chiswell, and S. Businger (1994), GPS/STORM-GPS sensing of atmospheric water vapor for meteorology, *J. Atmos. Oceanic Technol.*, *12*, 468–478.

Saastamoinen, J. (1972), Atmospheric correction for the troposphere and stratosphere in radio ranging of satellites, in *The Use of Artificial Satellites for Geodesy*, *Geophys. Monogr. Ser.*, 15, edited by S. W. Henriksen et al., pp. 247–251, AGU, Washington, D. C.

Saastamoinen, J. (1973a), Contribution to the theory of atmospheric refraction 1, *Bull. Geod.*, *105*, 279–298.

Saastamoinen, J. (1973b), Contribution to the theory of atmospheric refraction 2: Introduction to practical computation of astronomical refraction, *Bull. Geod.*, *106*, 383–397.

Saastamoinen, J. (1973c), Contribution to the theory of atmospheric refraction 3, *Bull. Geod.*, *107*, 13–34.

Smith, E., and S. Weintraub (1953), The constants in the equation for atmospheric refractive index at radio frequencies, *Proc. IRE*, 1035–1037.

Solheim, F., J. Vivekanandan, R. Ware, and C. Rocken (1999), Propagation delays induced in GPS signals by dry air, water vapor, hydrometeors, and other particulates, *J. Geophys. Res.*, *104*, 9663–9670.

Stein, J., E. Richard, J. Lafore, J. Pinty, N. Asencio, and S. Cosma (2000), High-resolution non-hydrostatic simulations of flash-flood episodes with grid-nesting and ice-phase parameterization, *Meteorol. Atmos. Phys.*, *72*, 203–221.

Stoew, B., and G. Elgered (2004), Characterization of atmospheric parameters using a ground based GPS network in north Europe, *J. Meteorol. Soc. Jpn.*, *82*, 587–596.

Thayer, D. (1974), An improved equation for the radio refractive index of air, *Radio Sci.*, *9*, 803–807.

Tregoning, P., R. Boers, D. O'Brien, and M. Hendy (1998), Accuracy of absolute precipitable water vapor estimates from GPS observations, *J. Geophys. Res.*, *103*, 28,701–28,710.

Vedel, H., K. Mogensen, and X.-Y. Huang (2001), Calculation of zenith delays from meteorological data comparison of NWP model, radiosonde and GPS delays, *Phys. Chem. Earth*, *26*, 497–502.

Vey, S., R. Dietrich, K.-P. Johnsen, J. Miao, and G. Heygster (2004), Comparison of tropospheric water vapour over Antarctica derived from AMSU-B data, ground-based GPS data and the NCEP/NCAR reanalysis, *J. Meteorol. Soc. Jpn.*, *82*, 259–267.

Yang, X., B. Sass, G. Elgered, J. M. Johansson, and T. Emardson (1999), A comparison of precipitable water vapour estimates by an NWP simulation and GPS observations, *J. Appl. Meteorol.*, *38*, 941–956.

H. Brenot, O. Caumont, and V. Ducrocq, CNRM/GMME/MICADO, Météo-France, F-31057 Toulouse, France. (hugues.brenot@obs.ujf-grenoble.fr)

C. Champollion, LDL, CNRS, Université de Montpellier II, F-34095 Montpellier, France.

A. Walpersdorf, LGIT, Maison des Géosciences, CNRS, Université Joseph Fourier, 1381 rue de la Piscine, F-38041 Grenoble, France.